University of Alberta

Stochastic Collocation Methods for Aeroelastic System with Uncertainty

By

Jian Deng

A thesis submitted in partial fulfillment of the

requirements for the degree of

Master of Science

In Applied Mathematics

Department of Mathematical and Statistical Sciences

Fall, 2009

Edmonton, Alberta

Examining Committee

Dr. Van Roessel, Henry, Department of Mathematical and Statistical Sciences (Chair)

Dr. Yau Shu Wong, Department of Mathematical and Statistical Sciences (Supervisor)

Dr. Christina Adela Popescu, Department of Mathematical and Statistical Sciences (Co-supervisor)

Dr. Zihui, Xia, Department of Mechanical Engineering

Abstract

Computation methods based on the Wiener chaos expansion have been developed to study the behaviors of the aeroelastic system with randomparameters. It is proven that the discrete wavelet transformation is one ofthe most accurate and efficient numerical schemes for this uncertainty quantizationproblem. In this thesis, we propose the stochastic collocation methods(SCM), whichis a type of sampling method combining the strength of the MonteCarlo simulation and the stochastic Galerkin method. The convergence with respect to the number of the nodal points is investigated, and simulation results to aeroelastic models in the presence of uncertainty in the system parameter and due to the initial condition are reported. It is demonstrated that the accuracy of the SCM is comparable to those achieved by using the wavelet chaos expansion. However, the SCM is more straightforward, efficient and easy to implement.

Acknowledgements

I am deeply indebted and appreciate to my supervisors Professor Yau Shu Wong and Professor Christina Adela Popescu, for their excellent guidance and great encouragement and generous support during my study at Edmonton.

I am truly grateful to the Department of Mathematical & Statistical Sciences, University of Alberta for its support through my master program.

I would like to thank many of my friends in Edmonton, such as Junfeng Ma and John Lang, for their enthusiastic help on my study and living in Edmonton. I also want to thank my officemates, Zhisheng Shuai, Aaron Lim and Fei Li, for the many happy conversations and laughter we had.

Finally, I am greatly indebted to my parents. Without their constant and selfless love and support, I could not have the opportunity to have and enjoy such joyous and great life in Canada.

List of Tables

List of Figures

Nomenclature

α	pitch angle of airfoil
$\delta_{j,l}$	Kronecker delta function
ϵ	error
η	non-dimensional plunge displacement of the elastic axis
$\mathcal{I}$	interpolation operator
$\mathcal{W}_N$	multidimensional wavelet functional subspace with total resolution level N
$\mathcal{W}_{\mu_i}$	one dimensional wavelet functional subspace with resolution level μ_i
$\phi(\tau)$	Wagner function
$\Phi(v)$	Haar function
ψ_1, ψ_2	constants in Wagner's function
$\Psi_i(x)$	general chaos basis
$\rho(\xi)$	probability density function of ξ
τ	non-dimensional time
$\tilde{\omega}$	frequency ratio
ξ, ξ_i	random variable
ζ_α, ζ_η	viscous damping ratios in pitch and plunge
$C_L(\tau)$	aerodynamic lift coefficient
$C_M(\tau)$	pitching moment coefficient
$F(\xi)$	probability distribution function of ξ
$G(\eta)$	structural nonlinearity in plunge
H_n	n-th order normalized Hermite polynomial
k_n	coefficient of n-th order term in $M(\alpha)$
$M(\alpha)$	structural nonlinearity in pitch
P_n	n-th order Hermite polynomial

r_α	radius of gyration about elastic axis
U^*	non-dimensional velocity
U_L^*	non-dimensional linear flutter speed
U^{LCO}	the bifurcation point where stable LCO fold for fifth order polynomial pitch restoring term
W_n^P	functional subspace constructed by n dimensional Hermite polynomial with highest P order
W^M	functional subspace constructed by M one dimensional Hermite polynomial ($= \{v : v \in span\{P_j(x)\}_{j=0}^M\}$)
W_t	Brownian motion
x_α	non-dimensional distance from elastic axis to center of mass
DOF	degree of freedom
DWT	discrete wavelet transform
LCO	limit cycle oscillation
MCS	Monte Carol Simulation
ODE	ordinary differential equation
PC	polynomial chaos
PDF	probability density function
RDE	random differential equation
SCM	stochastic collocation method
SDE	stochastic differential equation
SGM	stochastic Galerkin method
t	time
UQ	uncertainty quantification
WHa	Wiener-Haar

Contents

Chapter 1

Introduction

The ultimate purpose of mathematical models is to describe and predict the future behaviors of physical systems. Although differential equations have been successfully used to explain and predict the responses of physical events, the accuracy of the predictions usually relies on the correct estimation or the measurement of the values of system parameters, initial values or boundary conditions. It is well known that for dynamical systems, especially the nonlinear systems, a small uncertainty in input data may trigger non-negligible changes in the system output. For example, introducing a small perturbation on the left boundary condition of the Burgers' equation, the location of the transition can change significantly [21]. Such changes can not be captured by simulations based on the deterministic differential equation.

The study of the uncertainty quantification (UQ) is to investigate the impact due to errors in parameters and models, and subsequently, it provides more reliable predictions for practical problems [21]. This topic has received an increasing amount of attention in recent years, especially in the context of complex systems where mathematical models can serve only as simplified and reduced representation of the true system. Thus in order to fully understand the impact of uncertain parameters, it is imperative to incorporate the uncertainty into the models and other system parameters. Due to the 'uncertain' nature of the uncertainty, the most common approach is to regard the data uncertainty as random variables and transform the deterministic dynamical system into the random dynamical system.

Notice that, the random differential equation (RDE) is different with the stochastic differential equation (SDE). To illustrate the difference, we consider a deterministic

differential equation (1.1):

$$\begin{aligned} u'(t) &= -\alpha u, \quad t > 0 \\ u(0) &= u_0, \end{aligned} \tag{1.1}$$

where the coefficient α and initial condition u_0 are constants.

The SDE is a Ito or Stratonovich differential equation with respect to the Brownian motion. e.g. the dynamic system (1.1) with 'noise':

$$\begin{aligned} u' &= -\alpha u + \sigma(u,t)\dot{W}_t, \quad t > 0 \\ u(0) &= u_0. \end{aligned} \tag{1.2}$$

We can also consider the Brownian motion introduced to the parameter α,

$$\begin{aligned} u' &= -(\alpha_0 + \sigma(u,t)\dot{W}_t)u, \quad t > 0 \\ u(0) &= u_0, \end{aligned} \tag{1.3}$$

where W_t is the Brownian motion and other coefficients are constants. For the SDE, some analysis and numerical tools, such as the stochastic calculus, have been reported. However, developing efficient computational methods for SDE is still an active research topic[10].

Unlike SDE, RDE focuses on dynamical systems with random parameters which do not vary in the time domain. The RDE model resulting from the dynamical system (1.1) with random coefficient $\alpha(\xi)$ is given by

$$\begin{aligned} u' &= -\alpha(\xi)u, \quad t > 0 \\ u(0) &= u_0, \end{aligned} \tag{1.4}$$

where the coefficient α is a function of the random variable ξ with the probability density function ρ.

In this thesis, we study the solutions of the differential equation with random input. However, not only a one dimensional UQ problem with uncertainty in system parameter

is investigated, but we will also consider two dimensional UQ problems including cases with a random variables in the system parameter and in the initial condition. Similar with (1.4), a typical differential equation with two random inputs is defined as an example of a two dimensional UQ problem:

$$\begin{aligned} u'(t) &= -\alpha(\xi_1)u, \quad t > 0 \\ u(0) &= \beta(\xi_2), \end{aligned} \tag{1.5}$$

where ξ_1 and ξ_2 are independent real random variables with the probability density functions ρ_1 and ρ_2 on $[a_1, b_1]$ and $[a_2, b_2]$, respectively. Here the coefficient $\alpha(\xi_1)$ is assumed to be a function of ξ_1, and the initial value $\beta(\xi_2)$ is a function of ξ_2.

It should be noted that the problems being investigated in this thesis include dynamical systems represented by a coupled system of nonlinear differential equations, and an aeroelastic system modeling an oscillating airfoil in pitch and plunge motions. Here, we particularly focus on efficient and robust computational techniques for solving dynamical systems in the presence of uncertainty.

The Monte Carlo simulation (MCS) is one of the most popular numerical methods to solve differential equations with random input. The idea of MCS is to sample the randomness in RDEs, and solve the differential equation on each realizations. For each realization of randomness, it becomes a deterministic problem in which regular numerical methods can be employed. MCS is easy to apply to practical problems and has been widely used in the engineering community. The major drawback of the MCS is the slow convergence, where the convergent rate with K realizations is asymptotically around $1/\sqrt{K}$. Hence, it is important to develop efficient numerical methods which are capable of dealing with the UQ problems.

In the recent years, there was a growing interest in the polynomial chaos expansion for solving RDEs. According to the Cameron-Martin theorem, the polynomial chaos expansion can be applied to any stochastic process with finite second moment. By incorporating the polynomial chaos expansion with the finite element method, Ghanem

and Spanos [13] developed the Stochastic Galerkin method (SGM). In SGM, the random parameters or initial values and the solution of RDE are represented in a finite truncated form of the expansion. Using the Galerkin projection to the RDE on each orthogonal polynomial function, we have the equations within the framework of the finite element method and they can be solved numerically. The method has been verified to be very efficient for many problems, e.g., [16], [17].

However, for long-term integration or problems with discontinuity in the random space, the SGM method fails to converge after a short time, and increasing the polynomial order provides only small improvement in the convergence [19]. Hence the use of the local chaos expansion, namely the Wiener-Haar wavelet expansion, is proposed, and it is proven to be more accurate and efficient than the global chaos expansion [8]. Moreover, the discrete wavelet transform (DWT) was introduced by Pettit et al. [11] to replace the Galerkin projection, because it is difficult to generate the equation within the framework of the finite element method for practical problems. DWT with Mallat's pyramid algorithm is easy to implement and computationally efficient in generating the coefficients of wavelet basis.

In the present study, we focus on the stochastic collocation method (SCM). In SCM, we seek to satisfy the differential equations at a discrete set of points, called the 'nodes', in the corresponding random space, and utilize the Lagrange polynomial interpolation to approach the solution of SDE. The SGM is developed and has been tested to problems under investigation in this thesis. It has been demonstrated that accuracy of results with the SCM is comparable to those resulted using the DWT, when the same number of realizations is used by the two methods. On the other hand, it is a simple task to generate the Lagrange interpolation polynomial. Therefore, from the computational point of view, the SCM is more efficient and requires less computing time compared to the DWT.

For a deterministic problem, let $u_h(t)$ denote the numerical solution of a dynamic

system. Then the error $\epsilon(t)$ is defined by:

$$\epsilon(t) =\mid u(t) - u_h(t) \mid \tag{1.6}$$

where $u(t)$ is the exact solution. However, in RDE, it is not suitable to define the error by the difference of the realizations of the exact solution and the numerical one. In stochastic analysis, one definition of the error is given by:

$$\epsilon(t) = E[(u(t,\xi) - u_h(t,\xi))^2] = \int (u(t,\xi) - u_h(t,\xi))^2 \rho(\xi) \mathrm{d}\xi \tag{1.7}$$

where ξ is a random variable with the density function ρ, $u(t,\xi)$ is the exact solution and $u_h(t,\xi)$ is the numerical solution.

The thesis is organized as follows. In Chapter 2, we discuss computational methods for UQ problems, namely the MCS, Wiener chaos expansion and SGM. Chapter 3 presents numerical simulations for nonlinear dynamical systems in the presence of uncertainty. The simulation results clearly demonstrate the power and the effectness of the SCM method. Finally, concluding remarks are reported in Chapter 4.

Chapter 2

Computational Methods

In the beginning, we will adopt a probability framework to model the uncertainty of the coefficients in the differential equations. Suppose that the random variable ξ has the distribution function $F : \mathbb{R} \to [0, 1]$ defined by

$$F(x) = P(\xi \leq x). \quad x \in \mathbb{R} \tag{2.1}$$

If $F(x)$ is continuous and strictly increasing, then there exists a function $\rho : \mathbb{R} \to [0, \infty)$ such that $F(x) = \int_{-\infty}^{x} \rho(y)\mathrm{d}y$ for every $x \in \mathbb{R}$, and ξ is said to be continuous random variable with probability density function ρ. Based on the assumed properties of $F(x)$, it follows that for all $y \in [0, 1]$ there is a unique $x \in [a, b]$ such that $F(x) = y$, Consequently, we can define the one-to-one mapping

$$y \in [0, 1] \to x \equiv F^{-1}(y) \in [a, b] \tag{2.2}$$

For the multi-dimensional UQ problems, we assume that the parameters $(\xi_1, \xi_2, \ldots, \xi_n) \in \mathbb{R}^n, n > 1$ are independent random variables. We follow the notation of [21] and adopt a probability framework to model $\xi = (\xi_1, \xi_2, \ldots, \xi_n)$ as a n-variate random vector. Similar as above, we will also focus on continuous random variables.

Let $\rho_i : \Gamma_i \to \mathbb{R}^+$ be the probability density function of the random variable ξ_i, where $\Gamma_i \subset \mathbb{R}$ is the support of the random variable ξ_i for $i = 1, \ldots, n$. Then we have the joint probability density function of the random vector $\xi = (\xi_1, \xi_2, \ldots, \xi_n)$:

$$\rho(\xi) = \prod_{i=1}^{n} \rho_i(\xi_i), \tag{2.3}$$

The support of the random vector is

$$\Gamma \triangleq \prod_{i=1}^{n} \Gamma_i \subset \mathbb{R}^N, \tag{2.4}$$

We can do numerical approximations in the finite dimensional (n-dimensional) random space Γ. Naturally, the solution of random differential equation should be a stochastic process $u(t,\xi) : D \times \Gamma \to \mathbb{R}$, where D is the domain of t.

To describe the behavior of the stochastic process $u(t,\xi)$, some important statistical characteristic are introduced.

1. the expected value of the stochastic process, $u(t,\xi)$.

$$E[u(t,\xi)] = \int_{-\infty}^{\infty} u(t,y)\rho_t(y)\mathrm{d}y \tag{2.5}$$

2. the variance of the stochastic process.

$$Var(u(t,\xi)) = E[(u(t,\xi) - E[u(t,\xi)])^2] \tag{2.6}$$

In the next three section, we will discuss the Monte Carlo Simulation, the Wiener chaos expansion and the stochastic collocation method, for this type of random differential equations.

2.1 Monte Carlo Method

One of the most common method to solve differential equations with random input is the Monte Carlo simulation (MCS). The idea of the MCS is to sample the random input based on its probability distribution function. For each realization, the random differential equation becomes deterministic and is easy to solve it using regular numerical methods, such as the Runge-Kutta scheme or the finite element method.

2.1.1 Numerical Simulation

In the one dimension case (1.4), let $\xi^{(1)}, \xi^{(2)}, \ldots \xi^{(N)}$ be the sequence of the realization of the random input based on their probability distribution function, where N is the number of realizations.

For each realization of the random variables, the random differential equation became deterministic:

$$\begin{aligned} u'(t) &= -\alpha(\xi^{(i)})u, \quad t > 0 \\ u(0) &= u_0. \end{aligned} \tag{2.7}$$

Solving the differential equation, we have the deterministic solution $u(t;\xi^{(i)})$ for each sample.

For the two dimensional case (1.5), N coupled random variable $(\xi_1^{(1)}, \xi_2^{(1)})$, $(\xi_1^{(2)}, \xi_2^{(2)})$, ..., $(\xi_1^{(N)}, \xi_2^{(N)})$, are required.

Similar with the process in the one dimensional case, we have N deterministic differential equations

$$\begin{aligned} u'(t) &= -\alpha(\xi_1^{(i)})u, \quad t > 0 \\ u(0) &= \beta(\xi_2^{(i)}), \end{aligned} \tag{2.8}$$

The deterministic solution is $u(t;\xi_1^{(i)}, \xi_2^{(i)})$

After the simulation, we can estimate the statistical characteristic of the solution. For example, in the one dimensional problem we have:

1. the expected value of the random solution

$$E[u(t,\xi)] \approx \frac{1}{N}\sum_{i=1}^{N} u(t;\xi^{(i)}) \tag{2.9}$$

2. the variance of the random solution

$$\begin{aligned} Var(u(t,\xi)) &= E[(u(t,\xi) - E[u(t,\xi)])^2] \\ &\approx \frac{1}{N}\sum_{i=1}^{N}(u(t;\xi^{(i)}) - \frac{1}{N}\sum_{i=1}^{N} u(t;\xi^{(i)}))^2 \end{aligned} \tag{2.10}$$

MCS is easy to apply to different problems as it only requires the corresponding deterministic solver. However, from the central limit theorem it is well know that the convergent rate of MCS with N realizations is asymptotically around $1/\sqrt{N}$.

Theorem 2.1 (Central Limit Theorem) *Let* $(\Omega, \Sigma, \mathcal{P})$ *be a probability space and* $\xi^{(1)}$, $\xi^{(2)}$, ..., $\xi^{(n)}$ *be independent random variable defined on* Ω. *Assume the* $\xi^{(i)}$ *have a common distribution with finite expectation* m *and finite nonzero variance* σ^2. *Define* $S_n = \sum_{i=1}^{n} \xi^{(i)}$, *then*

$$\begin{aligned} \lim_{n\to\infty} P(\frac{S_n - E[S_n]}{\sqrt{Var(S_n)}} \leq x) &= \lim_{n\to\infty} P(\frac{S_n - nm}{\sigma\sqrt{n}} \leq x) \\ &= \phi_{0,1}(x) \end{aligned} \tag{2.11}$$

for each $x \in \mathbb{R}$, *where* $\phi_{0,1}$ *is the distribution function of* $N(0,1)$ *[14].*

The theorem can be expresses in other two natural versions, one for sums and another for averages.

Theorem 2.2 *For each* $x \in \mathbb{R}$

$$\lim_{n\to\infty} (P(S_n \leq x) - \phi_{nm,\sigma\sqrt{n}}(x)) = 0 \tag{2.12}$$

and

$$\lim_{n\to\infty} (P(\frac{S_n}{n} \leq x) - \phi_{m,\frac{\sigma}{\sqrt{n}}}(x)) = 0 \tag{2.13}$$

The central limit theorem guarantees the convergence of MCS and provide the following approximation for the error:

$$E[(\frac{S_n}{n} - m)^2] \approx \frac{\sigma}{\sqrt{n}}. \tag{2.14}$$

More precise, the convergence rate of MCS is $1/\sqrt{N \log\log N}$ by the law of the iterated logarithm [10], which is quite slow and typically a large number of realizations are required.

Some techniques have been developed to improve the speed of convergence of the MCS, e.g. latin hypercube sampling, quasi Monte Carlo, etc. But the usage of these methods is restricted by additional requirements, and the applications are often limited, [21]. Consequently other type of algorithms were developed by engineers and mathematicians. It has been proved that the stochastic Galerkin method, which is based on the global chaos expansion, is more efficient than the MCS for many problems.

2.2 Wiener chaos expansion

The Wiener chaos expansion was first introduced by Wiener, to approximate a Gaussian process with Hermite polynomial functionals. According to the Cameron-Martin theorem, any square integrable functional is the limit of a Hermite series [22]. Thus any process with finite second-order moments can be represented by a Hermite polynomials chaos expansion [22].

The Hermite chaos expansion can be used for the uncertainty quantification problems in practical applications. For example, inspired by the theory of the chaos expansion, Ghanem and Spanos combined the Hermite chaos expansion with a finite element method [13]. Mathematicians and engineers applied successfully the technique to many uncertainty quantification problems, e.g.,[16],[17], etc.

2.2.1 Hermite chaos expansion

Consider the random variable ξ on the real axis $\mathbb{R}$ with Gaussian density function,

$$\rho(x) = \frac{1}{\sqrt{2\pi}} e^{-\frac{x^2}{2}} \tag{2.15}$$

We can denote the Hilbert space of the square integrable function as

$$L^2(\mathbb{R}) = \{f(x) : \int_{-\infty}^{+\infty} f^2(x)\rho(x)\mathrm{d}x < \infty\} \tag{2.16}$$

The inner product of the Hilbert space is defined as

$$(f, g) = \int_{-\infty}^{+\infty} f(x)g(x)\rho(x)\mathrm{d}x \tag{2.17}$$

As ξ is a standard Gaussian random variable $N(0, 1)$, then

$$E[f(\xi)g(\xi)] = (f, g) = \int_{-\infty}^{+\infty} f(x)g(x)\rho(x)\mathrm{d}x \tag{2.18}$$

Now we can construct the Hermite orthogonal polynomial in the Hilbert functional space $L^2(\mathbb{R})$:

$$P_n(x) = (-1)^n e^{\frac{x^2}{2}} \frac{\mathrm{d}^n}{\mathrm{d}x^n}(e^{-\frac{x^2}{2}}), \quad n = 0, 1, 2, \ldots \tag{2.19}$$

P_n are orthogonal polynomials with respect to the Gaussian density.

$$(P_n, P_m) = \int_{-\infty}^{+\infty} P_n(x)P_m(x)\rho(x)\mathrm{d}x = \begin{cases} 0 & \text{if} \quad n \neq m \\ n! & \text{if} \quad n = m \end{cases} \tag{2.20}$$

with normalization factors $\sqrt{n!}$. Therefore the normalized orthogonal polynomials are defined as

$$H_n(x) = \frac{(-1)^n}{\sqrt{n!}} e^{\frac{x^2}{2}} \frac{\mathrm{d}^n}{\mathrm{d}x^n}(e^{-\frac{x^2}{2}}), \quad n = 0, 1, 2, \ldots \tag{2.21}$$

Because $H_0 = 1$, from (2.18), we have

$$E[H_n(\xi)] = (H_n, 1) = \int_{-\infty}^{+\infty} H_n(x)\rho(x)\mathrm{d}x = 0 \quad n \neq 0 \tag{2.22}$$

This means that the expected value of the Hermite polynomials of a standard Gaussian random variable is zero, when the order of the polynomial is nonzero.

Without proof, we provide the recurrence relation of the non-normalized Hermite polynomials [22]:

$$P_0(x) = 1; \quad P_1(x) = x; \quad P_n(x) = xP_{n-1}(x) - (n-1)P_{n-2}(x) \tag{2.23}$$

From the recurrence relation, the non-normalized Hermite polynomials can be generated as follows:

$$\begin{aligned} &P_0(x) = 1; \\ &P_1(x) = x; \\ &P_2(x) = x^2 - 1; \\ &P_3(x) = x^3 - 3x; \\ &\ldots \end{aligned} \tag{2.24}$$

Moreover, we can construct a subspace using a finite number M of orthogonal polynomials.

$$W^M \triangleq \{v : v \in span\{P_j(x)\}_{j=0}^{M}\} \tag{2.25}$$

It is well known [2] that $\{H_n(x)\}_0^\infty$ is a complete orthogonal basis in the Hilbert space $L^2(\mathbb{R})$, which means that the sequence of subspaces will converge to $L^2(\mathbb{R})$ as the number of the orthogonal polynomials go to infinity:

$$W^M \to L^2(\mathbb{R}) \quad \text{as} \quad M \to \infty. \tag{2.26}$$

Consequently, for a practical problem, the Hermite orthogonal polynomial can be used to represent any square-integrable function of a standard Gaussian random variable in a truncated form.

In the multiple variable case, we assume that ξ is the standard normal random variable vector with zero mean and unit variance, where the random variable vector $\xi = (\xi_1, \xi_2, \ldots, \xi_n)$ consists of n independent Gaussian random variables. We can construct the Hilbert functional space $L^2(\mathbb{R}^n)$ with respect to the random variable vector.

$$L^2(\mathbb{R}^n) = \{f(\mathbf{x}) : \int_{\mathbb{R}^n} f^2(\mathbf{x})\rho(\mathbf{x})\mathrm{d}\mathbf{x} < \infty\} \tag{2.27}$$

where $\mathbf{x} = (x_1, x_2, \ldots, x_n)$ and

$$\rho(\mathbf{x}) = \rho(x_1, x_2, \ldots, x_n) = (\frac{1}{\sqrt{2\pi}})^n exp(-\frac{x_1^2 + x_2^2 + \cdots + x_n^2}{2}) \tag{2.28}$$

is the n-dimensional Gaussian density function with zero mean and unit variance.

The inner product of the functional space is defined as before,

$$(f, g) = \int_{\mathbb{R}^n} f(\mathbf{x})g(\mathbf{x})\rho(\mathbf{x})\mathrm{d}x \tag{2.29}$$

Then the expressions of the Hermite polynomials are given by

$$P_k(x_1, x_2, \ldots, x_n) = (-1)^n e^{\frac{1}{2}\mathbf{x}^T\mathbf{x}} \frac{\mathrm{d}^k}{\mathrm{d}x_1 \cdots \mathrm{d}x_k} e^{-\frac{1}{2}\mathbf{x}^T\mathbf{x}}, \quad k = 0, 1, 2, \ldots \tag{2.30}$$

Because the Hermite polynomials are a complete orthogonal basis of $L^2(\mathbb{R}^n)$ [22], any

square integrable function $\chi(\xi)$, can be represented in the form

$$\begin{aligned}\chi(\xi) =& a_0 P_0 \\ &+ \sum_{i_1=1}^{\infty} a_{i_1} P_1(\xi_{i_1}) \\ &+ \sum_{i_1=1}^{\infty} \sum_{i_2=1}^{i_1} a_{i_1,i_2} P_2(\xi_{i_1}, \xi_{i_2}) \\ &+ \sum_{i_1=1}^{\infty} \sum_{i_2=1}^{i_1} \sum_{i_3=1}^{i_2} a_{i_1,i_2,i_3} P_3(\xi_{i_1}, \xi_{i_2}, \xi_{i_3}) \\ &\cdots\end{aligned} \tag{2.31}$$

For convenience, we can rewrite (2.31) as

$$\chi(\xi) = \sum_{j=0}^{\infty} \widehat{a}_j \Psi_j(\xi), \tag{2.32}$$

where there is a one-to-one correspondence between $P_n(\xi_1, \xi_2, \ldots, \xi_n)$ and $\Psi_j(\xi)$.

To apply the Hermite chaos expansion into a practical problem, we need to truncate the expansion (2.32) in the form of finite summation. We define the polynomial space in $\mathbb{R}^n$ as

$$W_n^P \triangleq \bigotimes_{m_1+\cdots+m_n \le P} W^{m_i} \tag{2.33}$$

The tensor product is over all possible combinations of subspace W^{m_i} satisfying $m_1 + \cdots + m_n \le P$. Hence, the total degree of the n-variate orthogonal polynomial basis in W_n^P is not over P.

Let $\{\Psi_j(\xi)\}$ be the orthogonal polynomial basis of W_n^P. Then $\Psi_j(\xi)$ is constructed as the product of the polynomial basis in each dimension, i.e.,

$$\Psi_j(\xi) = P_{k_1}(\xi_1) \cdots P_{k_n}(\xi_n), \quad k_1 + \cdots + k_n \le P, \tag{2.34}$$

where $\{P_{k_i}(\xi_i)\}$ is a Hermite polynomial basis of W^{m_i} with order k_i for $1 \le i \le n$. Thus, $\Psi_j(\xi)$ corresponds one-to-one to the combination of product of Hermite polynomial in (2.34), and the dimension of W_n^P [21] is

$$\dim(W_n^P) = \binom{n+P}{P} \tag{2.35}$$

Actually, we can construct a product polynomial space with the degree of the polynomial for each variable ξ_i being at most P. However, it will trigger $(P+1)^n$ basis functions, too many in practical computation, especially in a large dimensional case. So we will only focus on the space (2.33), which is used most widely in the stochastic computations [22].

As previous mentioned, a stochastic process with finite second moment, denoted $u(t,\xi)$, can be represented by the Hermite polynomials, and approximated by a finite summation, denoted as $u_M(t,\xi)$, i.e., for any $t \in D$

$$u(t,\xi) = \sum_{i=0}^{\infty} \hat{u}_i(t)\Psi_i(\xi) \approx u_M(t,\xi) = \sum_{i=0}^{M} \hat{u}_i(t)\Psi_i(\xi), \quad M = \binom{n+P}{P}, \tag{2.36}$$

where D is the domain of t and $\{\hat{u}_i\}$ are the Fourier coefficients defined as

$$\hat{u}_i(t) = \int u(t,\xi)\Psi_i(\xi)\rho(\xi)\mathrm{d}\xi = E[u(t,\xi)\Psi_i(\xi)], \quad 0 \le i \le M \tag{2.37}$$

The truncation in (2.36) can be considered as the orthogonal projection of $u(t,\xi)$ from $L^2(\mathbb{R}^n)$ onto W_n^P. The error can be defined as

$$\begin{aligned} \epsilon(t) &\triangleq \| u(t,\xi) - u_M(t,\xi) \|_{L^2(\mathbb{R}^n)} \\ &= \sqrt{\int (u(t,\xi) - u_M(t,\xi)^2 \rho(\xi))\mathrm{d}\xi} \\ &= \sqrt{E[(u(t,\xi) - u_M(t,\xi))^2]}, \end{aligned} \tag{2.38}$$

and it will converge to zero as the order of approximation P goes to infinity [2].

Moreover, it can be proved that the projection $u_M(t,\xi)$ has the smallest error in the functional space W_n^P [3]. In other words, $u_M(t,\xi)$ is the best approximation with polynomials of degree up to P, i.e., for any $t \in D$ and $u(t,\xi) \in L^2(\mathbb{R}^n)$,

$$\| u(t,\xi) - u_M(t,\xi) \|_{L^2(\mathbb{R}^n)} = \inf_{\Phi \in W_n^P} \| u(t,\xi) - \Phi \|_{L^2(\mathbb{R}^n)} \tag{2.39}$$

Since when the number of the terms M is sufficiently large the stochastic process $u(t,\xi)$ can be expressed in the truncated form $u_M(t,\xi)$, the statistical characteristic can be retrieved from the truncated expansion, $u_M(t,\xi)$.

1. Following (2.22) and (2.34), the expected value of $u(t, \mathbf{x})$ is estimated as:

$$\begin{aligned} E[u(t,\xi)] \approx E[u_M(t,\xi)] &= \int (\sum_{i=0}^{M} \hat{u}_i(t)\Psi_i(\xi))\rho(\xi)\mathrm{d}\xi \\ &= \sum_{i=0}^{M} \hat{u}_i(t) \int \Psi_i(\xi))\rho(\xi)\mathrm{d}\xi \\ &= \sum_{i=0}^{M} \hat{u}_i(t) E[\Psi_i(\xi))] \\ &= \hat{u}_0(t) \end{aligned} \tag{2.40}$$

2. Using the orthogonality of the functional basis, the variance of the solution can be approximated as

$$\begin{aligned} Var[u(t,\xi)] &= E[(u(t,\xi) - E[u(t,\xi)])^2] \\ &\approx E[(u_M(t,\xi) - E[u_M(t,\xi)])^2] \\ &= E[(u_M(t,\xi) - u_0(t,\xi))^2] \\ &= E[(\sum_{i=1}^{M} \hat{u}_i(t)\Psi_i(\xi))^2] \\ &= \sum_{i=1}^{M} \hat{u}_i^2(t) E[\Psi_i^2(\xi)]. \end{aligned} \tag{2.41}$$

If the polynomial basis $\Psi_i(\xi)$ is normalized and orthogonal, the estimation of variance of $u(t, \xi)$ can be further simplified as $\sum_{i=1}^{M} \hat{u}_i^2(t)$, as

$$(\Psi_i(\xi), \Psi_i(\xi)) = \int \Psi_i^2(\xi)\rho(\xi)\mathrm{d}\xi = E[\Psi_i^2(\xi)] = 1 \tag{2.42}$$

2.2.2 Global chaos expansion

It has been proved that the Hermite polynomial expansion can converge to any arbitrary stochastic processes with finite second moment, and has the optimal convergence rate for Gaussian processes [22]. However, for non-Gaussian processes, the convergence rate of the Hermite polynomial expansion substantially drops. Subsequently, the general polynomial chaos is constructed to recover the convergence rate.

Consider a set of polynomials $\{\Psi_i(x)\}$ and suppose that $\{\Psi_i(x)\}$ satisfy the following orthogonality condition with respect to the probability density function ρ of the random variable ξ with support Γ.

$$(\Psi_i, \Psi_j) = \int_\Gamma \Psi_i(x)\Psi_j(x)\rho(x)\mathrm{d}x = \begin{cases} 0 & \text{if} \quad n \neq m \\ h_i^2 & \text{if} \quad i = j \end{cases} \tag{2.43}$$

where $h_i^2 = \int_\Gamma \Psi_i^2(x)\rho(x)\mathrm{d}x$ is the normalization factor.

The probability density function ρ in the orthogonality relation (2.43) defines the type of the orthogonal polynomials $\{\Psi_i(x)\}$. In other words, there is one-to-one correspondence between the probability density function ρ and the type of chaos polynomials. For example, the uniform random variable, whose probability density function is constant, and (2.43) defines Legendre polynomials [22]; the Gaussian distribution density function corresponds to the Hermite polynomials, which were shown in the previous subsection.

If ξ is a discrete random variable on Γ with the weight function

$$w(x) = P(x = \xi) \quad \xi \in \Gamma, \tag{2.44}$$

the inner product definition will become

$$(\Psi_i, \Psi_j) = \sum_{x\in\Gamma} \Psi_i(x)\Psi_j(x)w(x) = \begin{cases} 0 & if \quad n \neq m \\ h_i^2 & if \quad i = j, \end{cases} \tag{2.45}$$

where the normalization factor is $h_i^2 = \sum_{x\in\Gamma} \Psi_i(x)\Psi_i(x)w(x)$.

So we can define orthogonal polynomials for discrete random variable, for example, the Poisson distribution corresponds to the Charlier polynomials; and the binomial distribution corresponds to Krawtchouk polynomials [22].

In Table 1, we have linked orthogonal polynomials to well known distributions. Moreover, an important class of general polynomial chaos, which guarantees the optimal convergence rate for different kinds of random input, can be expressed using the Askey scheme of hypergeometric polynomials [22].

Table 1: Table 1: Correspondence between the type of general polynomial chaos and the probability distribution [21]

	Distribution	General PC basis polynomial	Support
Continuous	Gaussian	Hermite	$(-\infty, \infty)$
	Gamma	Laguerre	$[0, \infty)$
	Beta	Jacobi	$[a, b]$
	Uniform	Legendre	$[a, b]$
Discrete	Poisson	Charlier	$\{0, 1, 2, \ldots\}$
	Binomial	Krawtchouk	$\{0, 1, 2, \ldots, N\}$
	Negative Binomial	Meixner	$\{0, 1, 2, \ldots\}$
	Hypergeometric	Hahn	$\{0, 1, 2, \ldots, N\}$

The construction of the global chaos expansion is not restricted to polynomials. Any type of complete functional basis can be used to represent stochastic processes. Recently, various global chaos expansion were developed, such as the Fourier chaos expansion [12], multi-element polynomial expansion [18], etc., for specific application problems.

2.2.3 Stochastic Galerkin Method

The global polynomial expansion provides an efficient way to express stochastic processes. Furthermore, based on the Hermite chaos expansion, the stochastic Galerkin method (SGM) was developed by Ghanem and Spanos. Because of many successful applications (e.g., [16] and [17]), the SGM became one of the most important numerical method in the uncertainty quantification problem. As an illustration, without struggling in the detailed explanation on the process, we use SGM to solve the previous ODE (1.4).

Applying the chaos expansion to the solution u and the parameter α, we get

$$u(t, \xi) = \sum_{i=1}^{M} \hat{u}_i(t)\Psi_i(\xi), \quad \alpha(\xi) = \sum_{i=1}^{M} \hat{\alpha}_i \Psi_i(\xi), \tag{2.46}$$

where $\{\Psi_i(\xi)\}$ are normalized orthogonal functions that form a basis of the space W^M.

Substituting these expansion into the Eq.(1.4), we obtain

$$\sum_{i=1}^{M} \hat{u}_i'(t)\Psi_i = -\sum_{i=1}^{M}\sum_{j=1}^{M} \Psi_i\Psi_j\hat{\alpha}_i\hat{u}_j(t). \tag{2.47}$$

A Galerkin projection onto each function in the basis produces a set of coupled ordinary differential equation:

$$\hat{u}_i'(t) = -\sum_{i=1}^{M}\sum_{j=1}^{M} e_{ij}\hat{\alpha}_i\hat{u}_j(t), \quad i = 1, \cdots, M, \tag{2.48}$$

where $e_{ij} = E[\Psi_i\Psi_i\Psi_j]$. To solve this system of coupled ODEs, a standard ODE solver, such as the Runge-Kutta scheme, can be employed. The convergence rate of polynomial chaos and the impact of non-optimal global polynomial chaos was studied in [22].

We can not apply the previous process to the random differential equation (1.5) directly because the initial value of the governing equation is random. First we apply the chaos expansion to α and β, and we get

$$\alpha(\xi_1) = \sum_{l=0}^{M} \hat{\alpha}_l\Psi_l(\xi_1), \quad \text{and} \quad \beta(\xi_2) = \sum_{k=0}^{M} \hat{\beta}_k\Psi_k(\xi_2). \tag{2.49}$$

The solution $u(t, \xi_1, \xi_2)$ is expressed in the finite truncated form:

$$u(t, \xi_1, \xi_2) = \sum_{i=0}^{M}\sum_{j=0}^{i} u_{i,j}(t)\Psi_{i-j}(\xi_1)\Psi_j(\xi_2). \tag{2.50}$$

Here $\{\Psi_i(\xi_1)\}$ and $\{\Psi_j(\xi_2)\}$ are normalized orthogonal bases.

From the initial condition in Eq. (1.5), combining (2.49) and (2.50), we have

$$\sum_{k=0}^{M} \hat{\beta}_k\Psi_k(\xi_2) = \sum_{i=0}^{M}\sum_{j=0}^{i} u_{i,j}(0)\Psi_{i-j}(\xi_1)\Psi_j(\xi_2). \tag{2.51}$$

Then we can do the Galerkin projection on each orthogonal function $\{\Psi_k(\xi_2)\}$, and get

$$\hat{\beta}_k = \sum_{i=k}^{M} u_{i,k}(0)\Psi_{i-k}(\xi_1) \quad \text{for each } k = 0, \ldots, M. \tag{2.52}$$

Doing Galerkin projection on each orthogonal function $\{\Psi_{i-k}(\xi_1)\}$,$k \leq i \leq M$, we have

$$\hat{\beta}_k < \Psi_{i-k}, 1 >=< \Psi_{i-k}, \hat{\beta}_k >= u_{i,k}(0). \tag{2.53}$$

Using (2.22), we have the following set of initial condition.

$$u_{i,k}(0) = \begin{cases} \hat{\beta}_k & \text{if } i = k \\ 0 & \text{if } i \neq k. \end{cases} \tag{2.54}$$

On the other hand, substituting (2.49) and (2.50) into the differential equation (1.5), we have

$$\sum_{i=0}^{M}\sum_{j=0}^{i} u'_{i,j}(t)\Psi_{i-j}(\xi_1)\Psi_j(\xi_2) = -\sum_{l=0}^{M}\sum_{i=0}^{M}\sum_{j=0}^{i} \hat{\alpha}_l u_{i,j}(t)\Psi_{i-j}(\xi_1)\Psi_l(\xi_1)\Psi_j(\xi_2). \tag{2.55}$$

The Galerkin projection on each orthogonal function $\{\Psi_k(\xi_2)\}$ implies,

$$\sum_{i=k}^{M} u'_{i,k}(t)\Psi_{i-k}(\xi_1) = -\sum_{l=0}^{M}\sum_{i=k}^{M} \hat{\alpha}_l u_{i,k}(t)\Psi_{i-k}(\xi_1)\Psi_l(\xi_1) \quad \text{for each } k = 0, \ldots, M. \tag{2.56}$$

Doing Galerkin projection on each orthogonal function $\{\Psi_{i-k}(\xi_1)\}$ for $i = k, \ldots, M$, we get

$$u'_{i,k}(t) = \sum_{l=0}^{M}\sum_{i=k}^{M} \hat{\alpha}_l e_{ilk} u_{i,k}(t) \quad \text{for each } k = 0, \ldots, M, \tag{2.57}$$

where $e_{ilk} = E[\Psi_{i-k}\Psi_{i-k}\Psi_l]$.

Thus, the UQ problem is transformed in the coupled deterministic equations (2.57) with initial condition (2.54).

2.2.4 Wiener-Haar wavelet expansion

It has been verified that the stochastic Galerkin method, which is based on the global chaos expansion, is more efficient than the MCS for many problems. However, when the problem involves long-term integration or discontinuity in the random space, this method fails to converge after a short time, and increasing the polynomial order helps

little the convergence [19]. Hence, the use of the local chaos expansion, Wiener-Haar wavelet expansion, was proposed, and it was proved to be more accurate and efficient than the global chaos expansion ([8])

The Haar scaling function is defined as

$$\phi(v) = \mathbf{I}_{[0,1)}(v) = \begin{cases} 1 & \text{if} \quad 0 \leq v < 1, \\ 0 & \text{otherwise}, \end{cases} \tag{2.58}$$

where $\mathbf{I}_{[0,1)}$ is the indicator function of $[0, 1)$. We can also define the scaled function with the scaling factor j and the sliding factor k:

$$\phi_{j,k} = 2^{j/2}\phi(2^j v - k), \tag{2.59}$$

where the scaling factor j is a positive integer and the sliding factor $k = 0, \ldots, 2^j - 1$.

Consider the functional space $V_j = span\{\phi_{j,k}, k \in [0, 2^j - 1]\}$ and denote the projection of the square-integrable function $f \in L^2$ onto the space V_j as $P^j f$. Hence we have

$$P^j f(v) = \sum_{k=0}^{2^j-1} f_{j,k}\phi_{j,k}(v), \tag{2.60}$$

where the coefficients are given by the inner product

$$f_{j,k} = \int_0^1 f(v)\phi_{j,k}(v)\mathrm{d}v. \tag{2.61}$$

The detail function $g^{j-1} \in V_j$ is defined as the difference between two resolution levels:

$$g^{j-1} = P^j f - P^{j-1} f. \tag{2.62}$$

To express the detail function, the Haar function $\Phi(v)$ is defined as:

$$\Phi(v) \triangleq \frac{1}{\sqrt{2}}(\phi_{1,0}(v) - \phi_{1,1}(v)) = \begin{cases} 1 & \text{if} \quad 0 \leq v < \frac{1}{2}, \\ -1 & \text{if} \quad \frac{1}{2} \leq v < 1, \\ 0 & \text{otherwise.} \end{cases} \tag{2.63}$$

Similar with (2.59), shifting and scaling the Haar function, we have

$$\Phi_{j,k}(v) = 2^{j/2}\Phi(2^j v - k), \quad j = 1, 2, \ldots, \text{and} \quad k = 0, \ldots, 2^j - 1 \tag{2.64}$$

We have the following properties of the functions $\{\Phi_{j,k}\}$

$$\begin{aligned} &\int_0^1 \Phi_{j,k}(v)\mathrm{d}v = 0 \quad \text{and} \quad \int_0^1 \Phi_{j,k}^2(v)\mathrm{d}v = 1 \\ &\int_0^1 \Phi_{j,k}(v)\Phi_{l,m}(v)\mathrm{d}v = 0 \quad \text{if} \quad j \neq l \quad \text{or} \quad k \neq m \end{aligned} \tag{2.65}$$

Consequently, $\{\Phi_{j,k}\}$ is a set of normalized orthogonal functions. Any square-integrable function $f \in L^2([0,1])$ can be expanded as

$$f = \sum_{j,k} d_{j,k}\Phi_{j,k}, \quad \text{with} \quad d_{j,k} = \int_0^1 f(v)\Phi_{j,k}(v)\mathrm{d}v. \tag{2.66}$$

Hence, the detail function g^{j-1} can be expressed as

$$g^{j-1} = \sum_{k=0}^{2^{j-1}-1} d_{j-1,k}\Phi_{j-1,k}(v). \tag{2.67}$$

From (2.62), we have

$$\begin{aligned} P^j f &= P^{j-1}f + \sum_{k=0}^{2^{j-1}-1} d_{j-1,k}\Phi_{j-1,k}(v) \\ &= P^{j-2}f + \sum_{k=0}^{2^{j-2}-1} d_{j-2,k}\Phi_{j-2,k}(v) + \sum_{k=0}^{2^j-1} d_{j-1,k}\Phi_{j-1,k}(v) \\ &\cdots \\ &= P^0 f + \sum_{i=1}^{j}\sum_{k=0}^{2^{i-1}-1} d_{i,k}\Phi_{i,k}(v) \\ &= c_0\phi(v) + \sum_{i=0}^{j-1}\sum_{k=0}^{2^i-1} d_{i,k}\Phi_{i,k}(v). \end{aligned} \tag{2.68}$$

For the stochastic analysis, let ξ be a continuous random variable on the finite interval $[a, b]$. On the assumption that the probability distribution function $F(\xi)$ is

continuous and strictly increasing, there exists the density function $\rho(x)$ for ξ and the inverse function of $F(x)$ such that $y \in [0,1] \to x \equiv F^{-1}(y) \in [a,b]$.

The stochastic process with finite second moment $u(t,\xi)$ can be represented in the form of the wavelet expansion

$$u(t,\xi) = u_0(t) + \sum_{j=0}^{\infty} \sum_{k=0}^{2^j-1} u_{j,k}(t) w_{j,k}(\xi), \tag{2.69}$$

where $u_{j,k}(t)$ are the coefficients of the wavelet approximation of $u(t,\xi)$, and $w_{j,k}(\xi) = \Phi_{j,k}(F(\xi))$. Hence we can rewrite (2.69) as

$$u(t,\xi) = u_0(t) + \sum_{j=0}^{\infty} \sum_{k=0}^{2^j-1} u_{j,k}(t) \Phi_{j,k}(F(\xi)). \tag{2.70}$$

Moreover, the Haar wavelet has the orthogonal properties for the density function ρ,

$$\int_a^b w_{j,k}(\xi) w_{l,m}(\xi) \rho(\xi) \mathrm{d}\xi = \int_0^1 \Phi_{j,k}(y) \Phi_{l,m}(y) \mathrm{d}(y) = \delta_{j,l} \delta_{k,m}, \tag{2.71}$$

where $\delta_{j,l}$ is the Kronecker delta function

$$\delta_{j,l} = \begin{cases} 1 & \text{if} \quad j = l \\ 0 & \text{if} \quad j \neq l. \end{cases} \tag{2.72}$$

This means that the wavelet functions $\{w_{j,k}, j = 1, 2, \ldots, \text{and} \quad k = 0, \ldots, 2^j - 1, \}$ form an orthogonal system with respect to the inner product

$$(f,g) = \int_a^b f(\xi) g(\xi) \rho(\xi) \mathrm{d}\xi. \tag{2.73}$$

In fact, $\{w_{j,k}, j = 1, 2, \ldots, \text{and} \quad k = 0, \ldots, 2^j - 1, \}$ is a complete orthogonal basis of $L^2([a,b])$, and it can represent any stochastic processes with finite-second moment [9].

2.2.5 Multidimensional Wavelet Basis

Following the notation in [8], we use a positive integer λ as the resolution level to combine the scaling factor j and the sliding factor k: $\lambda = 2^j + k$. Let $\triangledown$ be the set of

the resolution indexes, and let rewrite (2.70) as

$$u(t,\xi) = u_0(t) + \sum_{\lambda\in\nabla} u_{t,\lambda} w_\lambda(\xi). \tag{2.74}$$

We denote the functional subspace $\{g : g \in span\{w_\lambda\}_{\lambda=0}^{\mu}\}$ with finite resolution level by $\mathcal{W}_\mu$.

Let ξ be the random vector formed with the independent random variables $\xi = (\xi_1, \xi_2, \ldots, \xi_n)$. The multi-dimensional wavelet subspace is constructed as [8]

$$\mathcal{W}_N \triangleq \bigotimes_{\mu_1+\cdots+\mu_n\le N} \mathcal{W}_{\mu_i} \tag{2.75}$$

Then the stochastic processes $u(t,\xi)$ is expressed by the truncated form of the wavelet basis as

$$\begin{aligned} u(t,\xi) = u_0(t) &+ \sum_{i_1=1}^{N} u_{i_1}(t)\mathfrak{W}_1(\xi_i) \\ &+ \sum_{i_1=1}^{N}\sum_{i_2=1}^{i_1} u_{i_1,i_2}(t)\mathfrak{W}_2(\xi_{i_1},\xi_{i_2}) \\ &+ \sum_{i_1=1}^{N}\sum_{i_2=1}^{i_1}\sum_{i_3=1}^{i_2} u_{i_1,i_2,i_3}(t)\mathfrak{W}_3(\xi_{i_1},\xi_{i_2},\xi_{i_3}) + \cdots, \end{aligned} \tag{2.76}$$

where $\mathfrak{W}_i$ is the product of the functions in the wavelet basis on each dimension, i.e.,

$$\mathfrak{W}_i \in \{\prod_{k=1}^{i} w_{\mu_k} : \sum_{k=1}^{i}\mu_k \le N\}, \tag{2.77}$$

and $u_{i_1,i_2,\ldots}(t)$ are the coefficients of the expansion.

2.2.6 Discrete Wavelet Transform

In practice, the series (2.70) is truncated to a resolution level $j = J$:

$$u(t,\xi) \approx u_0(t) + \sum_{j=0}^{J}\sum_{k=0}^{2^j-1} u_{j,k}(t)\Phi_{j,k}(F(\xi)). \tag{2.78}$$

As the stochastic processes $u(t,\xi)$ is expressed in the truncated expansion given in (2.78), one way to determine the wavelet coefficients $u_{j,k}(t)$ is the Galerkin projection.

However, generating the explicit equations of the stochastic Galerkin projection is not a simple task for many practical problems.

An alternative is to evaluate the wavelet coefficients $u_{j,k}(t)$ using the Discrete Wavelet Transform (DWT). Because of the orthogonality of the wavelet basis (see (2.71)), the coefficients can be calculated as follows:

$$u_{j,k}(t) = \int_a^b u(t,\xi)\Phi_{j,k}(F(\xi))\rho(\xi)\mathrm{d}\xi = \int_0^1 u(t,F^{-1}(y))\Phi_{j,k}(y)\mathrm{d}y. \tag{2.79}$$

Instead of MCS or numerical integration, Mallat's pyramid algorithm for the DWT can be employed to compute the 2^{J+1} wavelet expansion coefficients [1]. This algorithm is much more computationally efficient and yields Wiener-Haar coefficients with significantly greater accuracy than MCS or numerical integration.

To determine the 2^{J+1} wavelet coefficient, Mallat's pyramid algorithm requires at least 2^{J+1} realization. Therefore the DWT can be considered as a type of 'sampling' method, and used to replace the Galerkin projection in order to overcome the difficulty of generating the explicit equations of the stochastic Galerkin projection.

2.3 Stochastic collocation method

In this thesis we propose to study the random dynamics using an approach based on the stochastic collocation method (SCM). Collocation method is a way to predict the behavior of the system at a fixed time by interpolation. Using interpolation instead of the DWT makes the SCM much more straightforward to implement and save the computational time for estimating the coefficients of the wavelet basis. Thus the selection of the interpolation methods is the essential part of the design of SCM.

2.3.1 Lagrange interpolation polynomial

Let us consider the sequence of the powers of x: $1, x, x^2, \ldots, x^n, \ldots$, and then form linear combinations of the first $n+1$ elements $\{x^i, i = 0, \ldots, n\}$ with real coefficients

c_i:

$$g(x) = c_0 + c_1 x + c_2 x^2 + \ldots + c_n x^n. \tag{2.80}$$

In the theory of interpolation, a certain finite number $n+1$ of points $x_0 < x_1 < \ldots < x_n$ belonging to the interval $[a, b]$ are selected, and for any real valued function f, a function $g(x)$ as in (2.80) is constructed such that it passes through the points $(x_i, f(x_i))$. In other words, we seek the coefficients c_i such that we have the following equalities:

$$f(x_i) = g(x_i) = c_0 + c_1 x_i + c_2 x_i^2 + \ldots + c_n x_i^n \quad i = 0, 1, 2, \ldots, n \tag{2.81}$$

Equation (2.81) can be seen as a linear system of $n+1$ equation with $n+1$ variables, $c_0, \ldots, c_n$. The determinant of the system is

$$A = \begin{vmatrix} 1 & x_0 & x_0^2 & \ldots & x_0^n \\ 1 & x_1 & x_1^2 & \ldots & x_1^n \\ \ldots & \ldots & \ldots & \ldots & \ldots \\ \ldots & \ldots & \ldots & \ldots & \ldots \\ 1 & x_n & x_n^2 & \ldots & x_n^n \end{vmatrix}.$$

This is a Vandermond determinant, and equals to $\prod_{i>j}(x_i - x_j)$ [4]. Therefore, based on the assumption that $x_i \neq x_j (i \neq j)$, the determinant is not zero, which implies that the solution $\{c_i\}$ of the system (2.81) is unique for $i = 1, \ldots, n$. Consequently the interpolation polynomial is determinated uniquely.

To determine the interpolation polynomial $g(x)$, we can express the interpolation function in the form:

$$g(x) = f(x_0)\delta_0(x) + f(x_1)\delta_1(x) + \cdots + f(x_n)\delta_n(x), \tag{2.82}$$

where $\delta_i(x)$ is called the Lagrange polynomial and determined by [4]

$$\delta_i(x) = \frac{(x - x_0)(x - x_1)\ldots(x - x_{i-1})(x - x_{i+1})\ldots(x - x_n)}{(x_i - x_0)(x_i - x_1)\ldots(x_i - x_{i-1})(x_i - x_{i+1})\ldots(x_i - x_n)}. \tag{2.83}$$

Notice that $\delta_i(x_j)$ is a linear combination of $1, x, x^2, \ldots, x^n$ satisfying

$$\delta_i(x_j) = \begin{cases} 1 & \text{if} \quad i = j \\ 0 & \text{if} \quad i \neq j, \end{cases} \tag{2.84}$$

Hence equation (2.82) can be expressed as

$$\begin{aligned} g(x) =& f(x_0)\frac{(x-x_1)\ldots(x-x_n)}{(x_0-x_1)\ldots(x_0-x_n)} \\ &+ f(x_1)\frac{(x-x_0)(x-x_2)\ldots(x-x_n)}{(x_1-x_0)(x_1-x_2)\ldots(x_1-x_n)} + \ldots \\ &+ f(x_n)\frac{(x-x_1)\ldots(x-x_{n-1})}{(x_n-x_0)(x_n-x_1)\ldots(x_n-x_{n-1})} \end{aligned} \tag{2.85}$$

This polynomial is called the Lagrange interpolation polynomial, and denoted by $L_n(x)$, where n is the degree of the polynomial.

Next we apply the interpolation on the equidistant points

$$x_1 - x_0 = x_2 - x_1 = \ldots = x_n - x_{n-1} = h. \tag{2.86}$$

Let $\frac{x-x_0}{h} = t$, and replacing in (2.83) we have

$$\begin{aligned} \delta_i(t) &= \frac{(-1)^{n-i}t(t-1)\ldots(t-i+1)(t-i-1)\ldots(t-n)}{i!(n-i)!} \\ &= \begin{cases} (-1)^{n-i}\binom{n}{i}\frac{t(t-1)\ldots(t-n)}{(t-i)n!}, & \text{if } t \neq i \\ 1, & \text{if } t = i \end{cases} \end{aligned} \tag{2.87}$$

Thus the Lagrange interpolation polynomial becomes

$$L_n(x_0 + th) = \begin{cases} \frac{t(t-1)\ldots(t-n)}{n!}\sum_{i=0}^{n}(-1)^{n-i}\binom{n}{i}\frac{f(x_i)}{(t-i)}, & \text{if } t \neq 1, 2, \ldots, n \\ f(x_i), & \text{if } t = 1, 2, \ldots, n. \end{cases} \tag{2.88}$$

Notice that the coefficients of $f(x_i)$ are independent of both $f_i(x)$ and h, and they can be used for any equidistant nodes.

Although the interpolation polynomial $g(x)$ coincides with the function f at the points $x_0, x_1, \ldots, x_n$, the polynomial $g(x)$ generally differs from the function $f(x)$ at

other points, except in the case when $f(x)$ is a polynomial of degree less than $n+1$. We call this kind of difference $\mid f(x) - L_n(x) \mid$ the error of the method [4].

To study the error of the method, we have to assume that the $f(x)$ is $n+1$ differentiable on the interval $[a, b]$. The error of the method is given by: [4]

$$f(x) - L_n(x) = \frac{f^{(n+1)}(\eta)}{(n+1)!}(x - x_0)(x - x_1)\dots(x - x_n), \tag{2.89}$$

where $\eta \in (a, b)$. If $f^{(n+1)}(x)$ is bounded, i.e., $M_{n+1} = \sup_{x\in[a,b]} \mid f^{(n+1)}(x) \mid < \infty$, then

$$\mid f(x) - L_n(x) \mid \leq \frac{M_{n+1}}{(n+1)!}(x - x_0)(x - x_0)\dots(x - x_n). \tag{2.90}$$

Due to the following theorem of Weierstrass, any continuous function can be approximated by a polynomial:

Theorem 2.3 *For any function $f \in C[a, b]$ and any $\varepsilon > 0$, there exists a polynomial P such that*

$$\mid P(x) - f(x) \mid \leq \varepsilon \quad \textit{for all } x \in [a, b]. \tag{2.91}$$

This might lead us to believe that error of the method can be reduced by increasing the number of nodes and the degree of the interpolation polynomial. However, a famous counter example was given by Runge:

$$f(x) = \frac{1}{1 + 25x^2}. \tag{2.92}$$

Even though this function is infinitely differentiable on $[-1, 1]$, the sequence of the interpolation polynomial $L_n(x)$ with equidistant nodes is divergent on this domain [15]. Hence the interpolation with equidistant nodes may fail to converge for a very smooth function. The nodes given by the Chebyshev abscissas can help to improve the convergence of the interpolation polynomials with high degree[15].

An alternative to interpolating with polynomials on selected nodes is to use piecewise polynomial functions on the interval [a,b]. Suppose that the selected nodes $a = x_0 < x_1 < \dots < x_n = b$ are allocated to some subintervals $[x_0, x_{i_1}], [x_{i_1}, x_{i_2}], \dots, [x_{i_k}, x_n]$,

where $i_1, i_2, \ldots, i_k$ are positive integers and $0 < i_1 < i_2 < \cdots < i_k < n$. Then the piecewise polynomial interpolation will be

$$g(x) = \begin{cases} L_{n_1}(x), & x \in [x_0, x_{i_1}) \\ L_{n_2}(x), & x \in [x_{i_1}, x_{i_2}) \\ \vdots & \\ L_{n_k}(x), & x \in [x_{i_k}, x_n], \end{cases} \tag{2.93}$$

where $L_{n_j}(x)$ is the interpolation polynomial with degree n_j on the interval $[x_{i_j}, x_{i_{j+1}})$. If the subintervals are arranged as $[x_0, x_1], [x_1, x_2], \ldots, [x_{n-1}, x_n]$ (i.e., only two nodes in each subinterval), the degree of the interpolation polynomial reduces to one, and a piecewise linear function is used in the interpolation:

$$\begin{aligned} &g(x) = f(x_i)\frac{x - x_{i+1}}{x_i - x_{i+1}} + f(x_{i+1})\frac{x - x_i}{x_{i+1} - x_i}, \quad \text{if} \quad x \in [x_i, x_{i+1}] \\ &\text{for} \quad i = 0, \ldots, n-1. \end{aligned} \tag{2.94}$$

Therefore the piecewise linear function can be expressed as

$$g(x) = \sum_{i=0}^{n} f(x_i) w_i(x) \tag{2.95}$$

where

$$w_1(x) = \begin{cases} \frac{x - x_1}{x_0 - x_1}, & x \in [x_0, x_1] \\ 0 & \text{otherwise,} \end{cases} \quad w_n(x) = \begin{cases} \frac{x - x_{n-1}}{x_n - x_{n-1}} & x \in [x_{n-1}, x_n] \\ 0 & \text{otherwise} \end{cases} \tag{2.96}$$

and

$$w_i(x) = \begin{cases} \frac{x - x_{i-1}}{x_i - x_{i-1}} & x \in [x_{i-1}, x_i] \\ \frac{x - x_{i+1}}{x_i - x_{i+1}}, & x \in [x_i, x_{i+1}] \\ 0 & \text{otherwise} \end{cases} \quad \text{for} \quad i = 2, \ldots, n-1. \tag{2.97}$$

The assumptions about the continuity of predicted function f may be not suitable in the UQ problem because of jump phenomena in the bifurcation of the governing equations. The discontinuity of f can make the convergence of high degree interpolation

polynomials very slow, or even impossible (e.g. because of the Gibbs' phenomenon [15]). Consequently, in our implementation of the SCM we use the piecewise interpolation with polynomial of degree 1.

2.3.2 Tensor products

To extend the one-dimensional interpolation to the multidimensional space, a natural way is to use the tensor products of one dimensional interpolations. For a real value function $f : [a, b]^n \to \mathbb{R}$, we can construct an one dimensional interpolation in each dimension by using the technique presented in the previous subsection:

$$\mathcal{I}^i f = \sum_{k=1}^{m_i} f(x_k^{(i)}) \delta_k(x^{(i)}). \tag{2.98}$$

Here the nodal sets are $\Theta_i = (x_1^{(i)}, x_2^{(i)}, \ldots, x_{m_i}^{(i)}) \subset [a, b]$, and $\mathcal{I}^i$ is the interpolation operator of f on the $i - th$ dimension. The tensor product for the multidimensional space is constructed as

$$\mathcal{I} f \equiv \bigotimes_{i=1}^{n} (\mathcal{I}^i(f)) \tag{2.99}$$

on the nodal set $\Theta = \bigotimes_{i=1}^{n} \Theta_i$. Thus the tensor product formula becomes the product of the one dimensional interpolation formula (2.98),

$$\mathcal{I} f = \sum_{k_1=1}^{m_1} \cdots \sum_{k_n=1}^{m_n} f(x_{k_1}^{(1)}, \ldots, x_{k_n}^{(n)}) \delta_{k_1}(x^{(1)}) \cdot \cdots \cdot \delta_{k_n}(x^{(n)}). \tag{2.100}$$

The computational complexity of SCM is N times that of the deterministic problem, where N is the number of nodal points. Therefore the total number of collocation points is one of the most important factor on the computational complexity of SCM.

In the tensor products, the number of nodes is $\mid \Theta \mid = m_1 \cdot \cdots \cdot m_n$. If the number of nodes in each dimension is the same, $m_1 = m_2 = \cdots = m_n \equiv m$, the total number of nodes become $N = m^n$. This number will grow exponentially with the increasing of dimension n. Because of the rapid growth of the number of nodes in high dimensions, the tensor product approach is mostly used at lower dimensions, for $n \leq 5$. In the

recent years, some technique of selecting nodes, such as sparse grids and Stroud's cubature [20] were developed to reduce the number of nodes in high dimensions and to improve the efficiency of SCM.

The problem studied here is restricted to the 2 dimensional random space. The 'curse of dimension' is still not obvious, and the number of the collocation points is acceptable in the practical computation. So we will focus on the tensor products for the 2 dimensional problem.

2.3.3 Numerical Implementation

Let $\Theta = \{\xi^{(i)}\}_{i=1}^{N} \in [a, b]$ be a set of nodes selected on the interval $[a, b]$, where N is the number of nodes. By requiring that (1.4) is satisfied in each nodes for any $k = 1, \ldots, N$, we obtain:

$$\begin{aligned} u'(t) &= -\alpha(\xi^{(k)})u, \quad t > 0 \\ u(0) &= u_0. \end{aligned} \tag{2.101}$$

We can estimate the solution $u(t, \xi)$ by a piecewise linear function (2.95):

$$\mathcal{I}u(t, \xi) = \sum_{k=0}^{N} \widetilde{u_k}(t) w_k(\xi), \text{ for all } t > 0, \tag{2.102}$$

where

$$\widetilde{u_k}(t) \triangleq u(t; \xi^{(k)}), \quad k = 1, \ldots, N, \tag{2.103}$$

is the value of the solution u at the given node $\xi^{(k)} \in \Theta$.

Thus the SCM is equivalent to solving N deterministic problems in each 'realization' of the random variables $\xi^{(k)}$ for $k = 1, \ldots, N$ [21].

We also present the SCM for Eq.(1.5). We select the nodes $\Theta = (\xi_1^{(1)}, \xi_1^{(2)}, \ldots, \xi_1^{(N_1)}) \times (\xi_2^{(1)}, \xi_2^{(2)}, \ldots, \xi_2^{(N_2)}) \in [a_1, b_1] \times [a_2, b_2]$. Since the equation (1.5) should be satisfied at the nodes Θ, we have

$$\begin{aligned} u'(t) &= -\alpha(\xi_1^{(i)})u, \quad t > 0 \\ u(0) &= \beta(\xi_2^{(j)}). \end{aligned} \tag{2.104}$$

The solution u is approximated by the tensor product interpolation polynomial

$$\mathcal{I}u(t,\xi_1,\xi_2) = \sum_{i=1}^{N_1}\sum_{j=1}^{N_2} \widetilde{u_{ij}}(t) w_i(\xi_1) w_j(\xi_2), \text{ for all } t > 0. \tag{2.105}$$

Here

$$\widetilde{u_{ij}}(t) \triangleq u(t;\xi_1^{(i)},\xi_2^{(j)}), \quad 1 \le i,j \le N. \tag{2.106}$$

Once we obtain the numerical solution of (1.4) or (1.5) at all collocation points, the expectation and variance can be evaluated to estimate the behavior of the system.

1. Using the estimation of the solution, $\mathcal{I}u(t,\xi)$, we can evaluate the expectation:

$$E[u(t,\xi)] \approx E[\mathcal{I}u(t,\xi)] = \sum_{k=1}^{N} u(t;\xi^{(k)}) \int_a^b w_k(\xi)\rho(\xi)\mathrm{d}\xi. \tag{2.107}$$

2. The variance of $u(t,\xi)$ is estimated as

$$E[(u(t,\xi) - E[u(t,\xi)])^2] \approx E[(\mathcal{I}u(t,\xi) - E[\mathcal{I}u(t,\xi)])^2]. \tag{2.108}$$

Chapter 3

Numerical Simulations

In this chapter, we evaluate the developed SCM and report simulation results using the SCM to study nonlinear dynamical systems with uncertainty due to the system parameters and the initial conditions. First, we consider two test models which were investigated in detail by Pettit and Beran [11], in which the Polynominal Chaos (PC) with Wiener Hermite expansion and Wiener Haar expansion were used to study the stochastic problems with oscillatory behaviors. Once the performance of the SCM is verified, we apply the SCM to investigate the Hopf bifurcation and the secondary bifurcation in an aeroelastic system.

3.1 Test Models

3.1.1 Sinusoidal model

Consider a sinusoidal stochastic process [11]

$$u(t,\xi) = sin(\omega(\xi)t), \tag{3.1}$$

where the random frequency $\omega = \omega_0 + \sigma_\omega(\xi - 0.5)$, ξ is a uniform random variable on $\Gamma = [0,1]$, $\omega_0 = 2\pi$, $\sigma_\omega/\omega_0 = 0.60$, and t = [0,10]. In order to test the convergence of the SCM, in our experiments, we applied 32 and 64 collocation nodes respectively.

In Fig. 1, we compare the expected values resulting from the SCM with 32, 64 nodes and those using the MCS with 10000 samples. In theory, the absolute value of

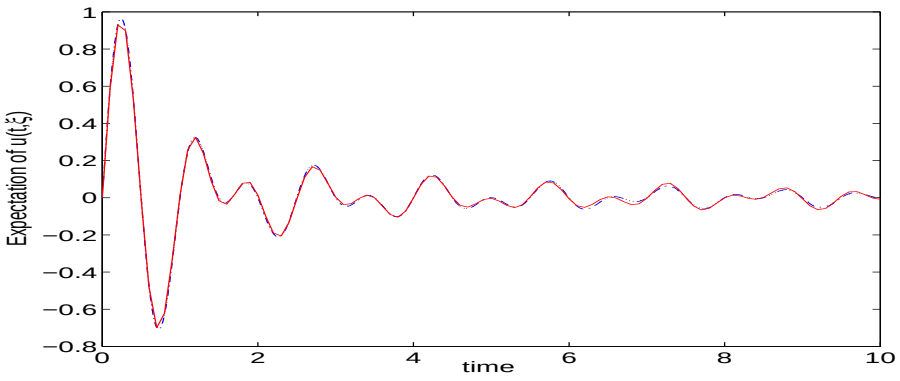

Figure 1: The evolution of $E[u(t,\xi)]$: Red - : MCS; Blue -. : SCM with 64 nodes; Black .. : SCM with 32 nodes

the expectation is bounded by $\frac{2}{\sigma_\omega t}$:

$$\begin{aligned} \mid E[u(t,\xi)] \mid &= \mid E[sin((\omega_0+\sigma_\omega(\xi-0.5))t)] \mid \\ &= \mid E[sin(\omega_0 t)cos(\sigma_\omega(\xi-0.5)t)] + E[cos(\omega_0 t)sin(\sigma_\omega(\xi-0.5)t)] \mid \\ &= \mid sin(\omega_0 t)E[cos(\sigma_\omega(\xi-0.5)t)] + cos(\omega_0 t)E[sin(\sigma_\omega(\xi-0.5)t)] \mid \\ &= \mid \frac{2sin(\omega_0 t)sin(\frac{\sigma_\omega t}{2})}{\sigma_\omega t} \mid \leq \frac{2}{\sigma_\omega t}, \end{aligned} \tag{3.2}$$

since $sin(x)$ is an odd function on $[-\frac{\sigma_\omega t}{2}, \frac{\sigma_\omega t}{2}]$.

Clearly, the SCM produces a good approximation to the oscillatory dynamics. In Fig. 2, we illustrate the plots showing $x(t)$ versus ξ at $t = 1, 2, ..., 10$. From the results shown in Figs 2, we observe that the SCM give excellent agreements for the model $u(t,\xi) = sin(\omega(\xi)t)$ for a fixed t. Thus, the piecewise linear interpolation on the nodal points is sufficient to provide a good estimation for the sinusoidal process. The accuracy of the realization for SCM depends on the collocation nodes. Fig. 3 shows the realization for SCM in the random space. A slight decay is observed for the SCM with 32 nodes.

The same sinusoidal model was used in [11] to study the performance of the polynomial chaos (PC) with Wiener-Hermite expansion. It was noted that the accuracy of the approximation is very sensitive to the order of the truncated PC expansion. Generally speaking, the order of the PC expansion should increase rapidly in order to

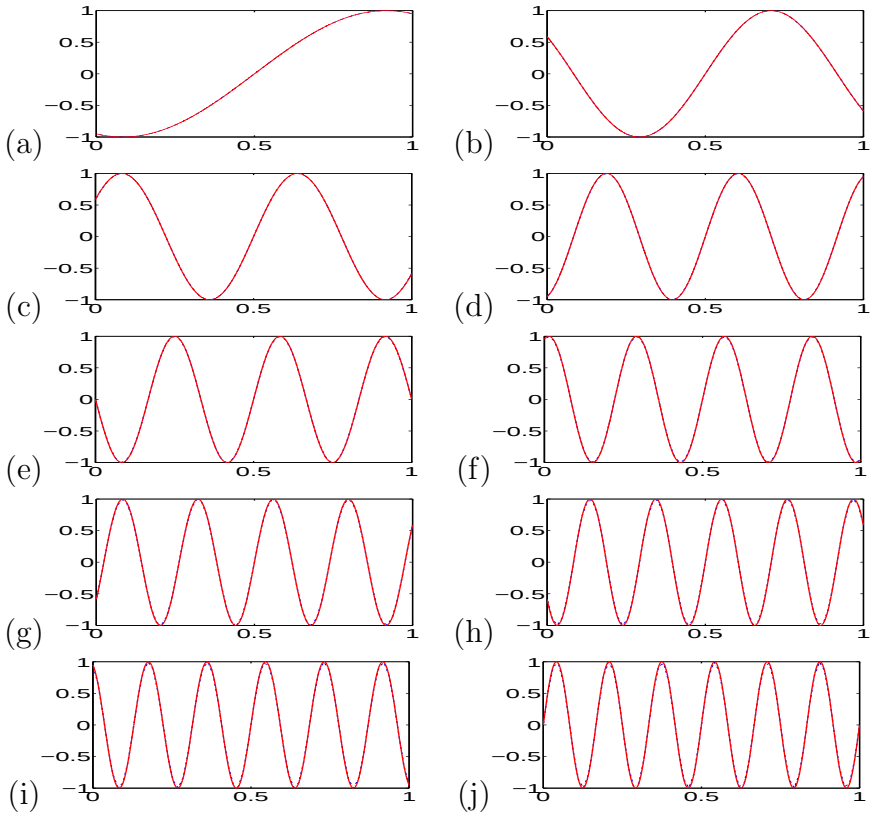

Figure 2: Estimated value of $u(t)$ versus ξ at $t = 1, \ldots, 10$ from (a) to (j). Red -: exact; Blue -.: SCM with 64 nodes

keep pace with the increasing frequency (see Fig. 2). Otherwise, the PC expansion fails to capture the correct oscillatory response after some time. The realizations of the sinusoidal random process based on the 10th-order Wiener Legendre expansions were reported in [11] and the problems were clearly noted for $t > 5$ (see Fig. 8 in [11]).

Therefore, by comparing the realizations from SCM (Fig. 3) and the PC expansion (Fig. 8 in [11]), we conclude that the SCM is superior to the PC expansion for long time integration for the sinusoidal model. However, due to the increasing frequency in the random space, the estimated expected value using SCM with 32 nodes fails at the later time $t > 40$ (see Fig. 4). To overcome the difficulty, more nodal points can be used in the SCM. Fig. 4 shows an excellent agreement for the SCM with 64 nodes and the MCS for time $t = [0, 70]$.

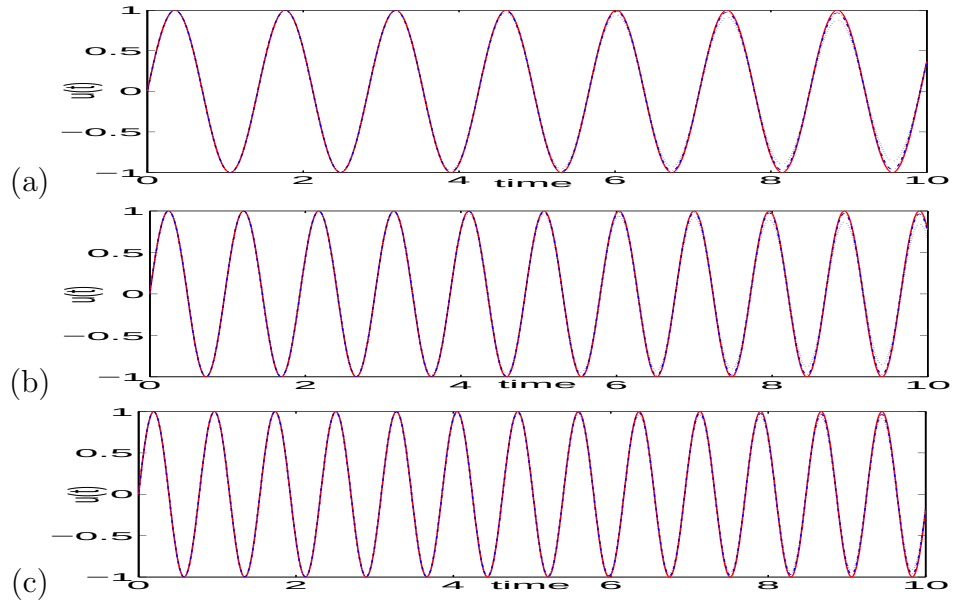

Figure 3: Three sample realizations for the SCM: Red - : exact ; Blue -. : SCM with 64 nodes; Black .. : SCM with 32 nodes; (a) for $\xi = 0.01$; (b) for $\xi = 0.56$; (c) for $\xi = 0.995$

3.1.2 Nonlinear dynamical system

The second test model is given by a nonlinear dynamical system with the following governing equations:

$$\begin{aligned} x' &= c_1 x + c_2 y + c_3 x y^2 + c_4 x^5 \\ y' &= c_5 x + c_6 y + c_7 y^3 + c_8 y^5 \end{aligned} \tag{3.3}$$

where $c_1 = c_6 = -0.2, c_2 = -1, c_3 = 1, c_4 = c_8 = -0.25, c_5 = 1$ and $c_7 = 0.5 + 0.5\xi$. The initial conditions are $x(0) = y(0) = 0.6$, and ξ is a uniform random variable on [0,1]. This system was studied in [11] to evaluate the performance of the PC with the Wiener Harr expansion in which the Hermite polynominal is replaced by the Haar wavelet series. Here, we employ the ode45 algorithm in Matlab 6.5, (which is the adaptive 4th/5th-order Runge-Kutta scheme with error checking as our deterministic solver in the SCM). If the estimated error is larger than the tolerance, the algotithm will refine the time step to retain the accuracy. The relative tolerance and absolute

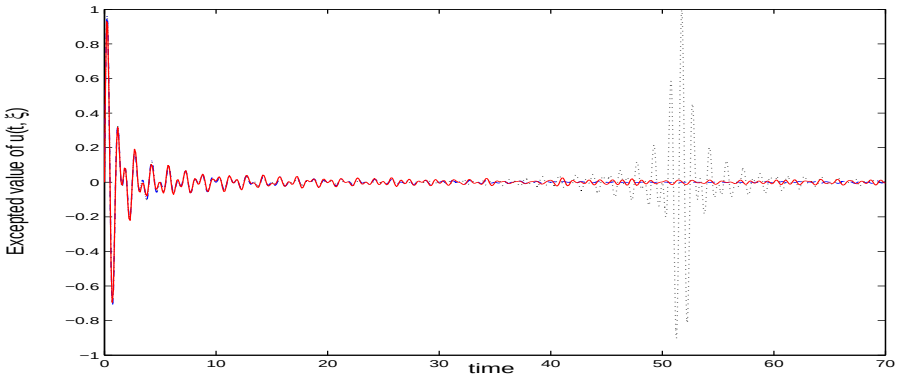

Figure 4: The loss of accuracy for the approximation to the expected value: Red - : MCS; Blue -. : SCM with 64 nodes; Black .. : SCM with 32 nodes

tolerance is set to 10^{-3}.

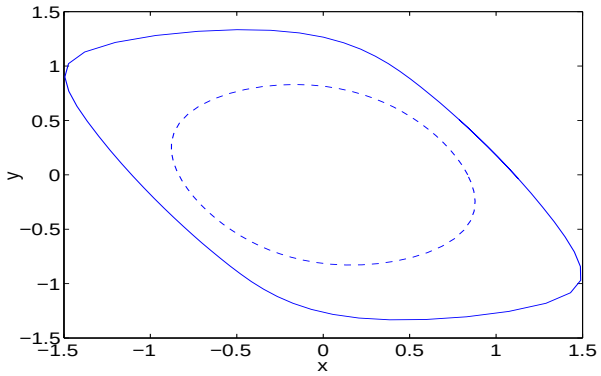

Figure 5: The limit cycles for $c_7 = 0.75$, solid line: stable limit cycle; dashed line: unstable limit cycle

In the dynamical system, there exists a stable limit cycle oscillation (LCO) and an unstable LCO (Fig. 5). When the initial point is inside the unstable LCO, the dynamic system converges to the equilibrium, namely zero. If the dynamic system starts with an initial point outside the unstable limit cycle, the system converges to the stable LCO. Numerical simulation shows that the occurrence and the amplitude of LCO is sensitive to the parameter c_7 [11]. Thus, it is of interest to investigate the system response with the uncertainty due to the coefficient c_7.

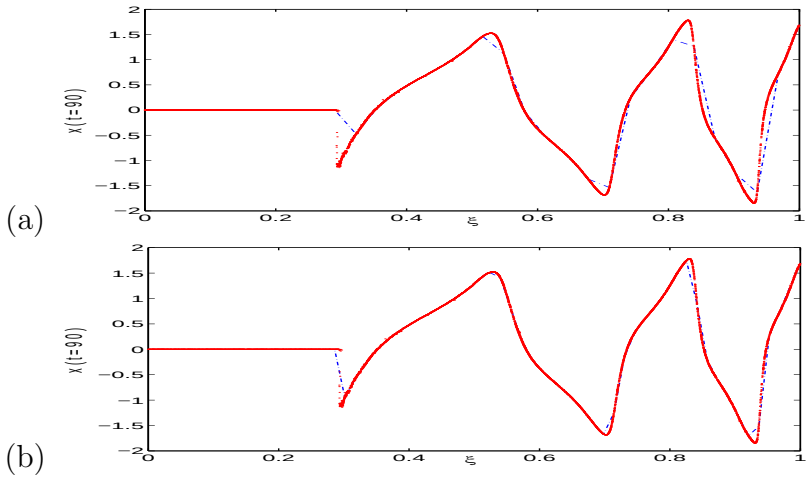

Figure 6: Simulation of $x(t)$ at $t = 90$, red dot: deterministic; blue dashed line: SCM with 32 nodes in (a) and 64 nodes in (b)

The random dynamical system under consideration exhibits a subcritical Hopf bifurcation, and it admits a discontinuity in the random space. Fig. 6 shows the simulation of $x(t)$ at $t = 90.00$, a time that is sufficiently large to allow the system to converges to LCO or zero. The discontinuity is detected at around $\xi^* = 0.3$. When ξ is less than ξ^*, the system converges to zero implying the initial point $(0.6, 0.6)$ is inside the unstable LCO. On the other hand, when ξ is greater than ξ^*, the system produces a LCO, and the initial point is outside the unstable LCO.

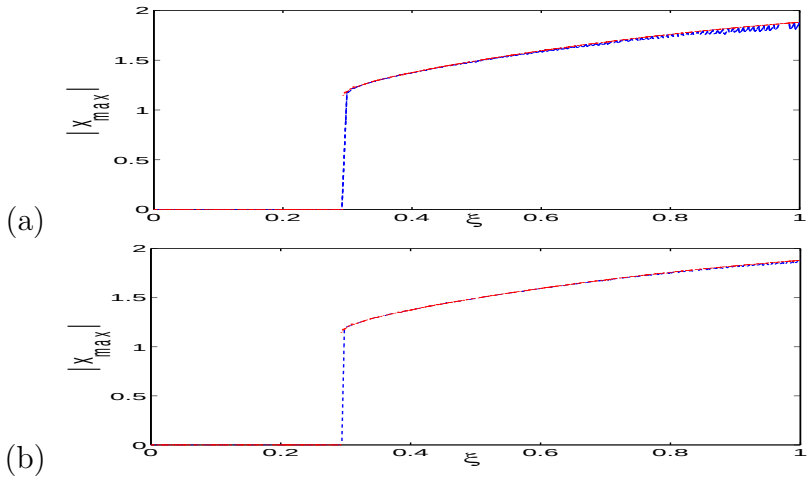

Figure 7: Maximum value of $|x(t)|$ for $t \geq 80$, red dot: deterministic; blue dashed line: SCM with 128 nodes in (a) and 256 nodes in (b)

When ξ is greater than the discontinuity ξ^*, some errors in the estimated peak value of $x(t = 90, \xi)$ are observed in Fig. 6. It means that the interpolation underestimates the peak value of the LCO. The error due to the interpolation on different time steps yields the decay of the amplitude of realization from the SCM (see Fig. 7), where the amplitude is defined by the maximum value of $|x|$ for $t \in [80, 100]$, which was chosen to allow the system to have sufficient time to converge to LCO or zero. However, from the plots presented in Fig. 6 and Fig. 7, more accurate results are obtained by introducing more nodal points in the SCM.

In Fig. 8, we estimate the probability density function of $x(t)$ at $t = 90.00$ by MCS with 10,000 simulations. It clearly shows that the SCM has an excellent agreement with the result based on the MCS. Moreover, the peak of the estimated probability density function represents well the probability that the dynamic system converges to zero.

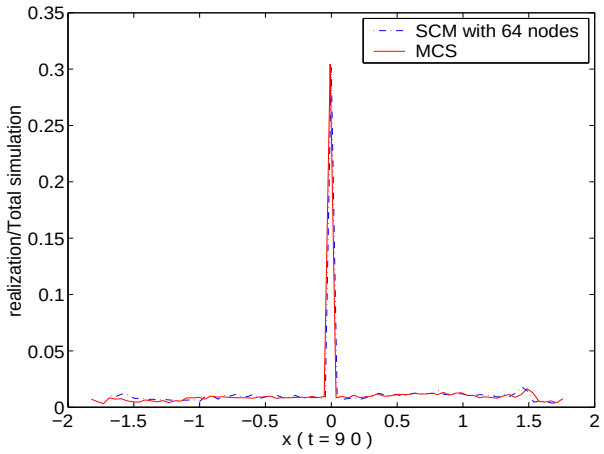

Figure 8: The density function of $x(t)$ at $t = 90.00$

For the dynamic system with random LCO, we also investigate the realization from SCM with 64 nodes for time $t = [0, 100]$. Fig. 9 and 10 display the realizations generated for $\xi = 0.682$ and $\xi = 0.780$, respectively, for which the system converges to the stable LCO. Using the same definition as introduced in [11]. the error of the

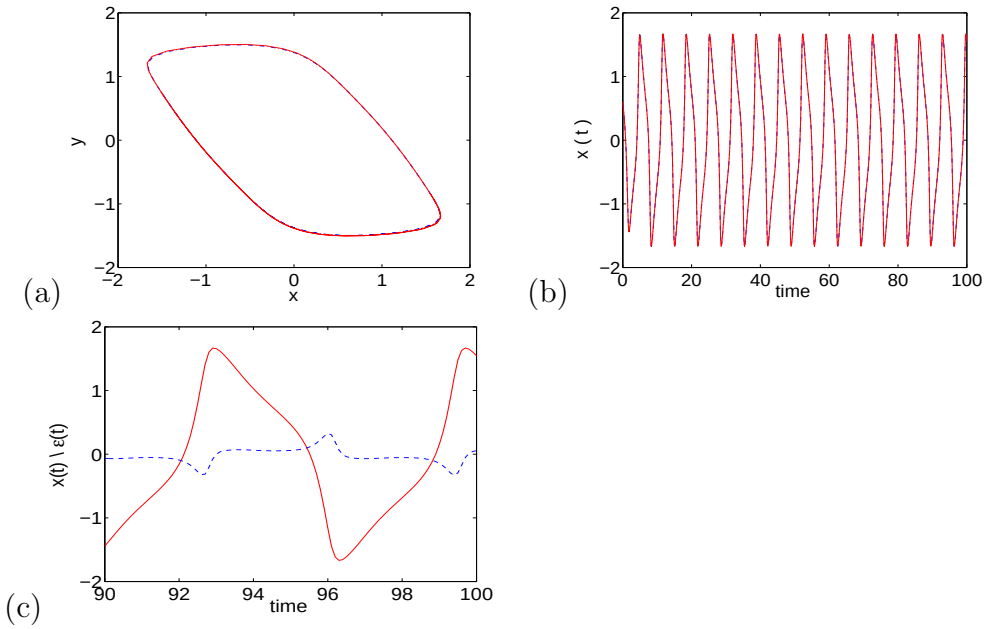

Figure 9: Comparision of full model and SCM with 64 nodes for $\xi = 0.682$: (a) phase plane plot of limit cycle, (b) realization, (c) detail on $[90, 100]$, when red - : deterministic in (a-c), blue -. : SCM in (a,b), and blue: error ε in (c)

realization is defined as

$$\varepsilon(t, \xi) = x_{approx}(t, \xi) - x(t, \xi) \tag{3.4}$$

where $x_{approx}(t, \xi)$ is the realization, and $x(t, \xi)$ is the solution from the deterministic system. The phase plane plots show that realizations from SCM accurately capture the LCO of the dynamic system. However, a small decay of the amplitude for $\xi = 0.780$ can be observed in Fig. 10 (a). It should be clear that the collocation nodes used in the SCM are uniformly selected, and do not include $\xi = 0.682$ and $\xi = 0.780$.

In [11], the realizations based on the Wiener-Haar (WHa) expansion for the stochastic model with $\xi = 0.682$ and $\xi = 0.780$ were reported (Figs.19 and 20 in [11]). The resolution level of the wavelet basis is 5, and 64 samples are included. The simulation results in [11] illustrated that the local wavelet expansion represents the oscillation on the stable LCO. However, when $\xi = 0.780$, there exists a time delay on the realization, consequently it yields a large error as defined as in (3.4). Therefore, we conclude that the performance of SCM shown in Fig 9 is as good as the local wavelet expansion for

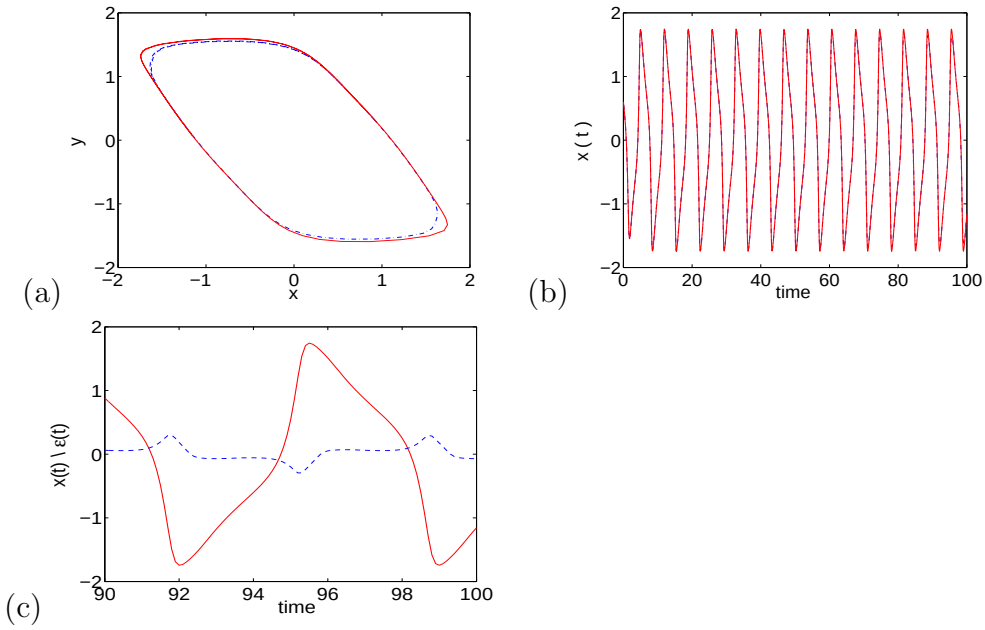

Figure 10: Comparision of full model and SCM with 64 nodes for $\xi = 0.780$: (a) phase plane plot of limit cycle, (b) realization, (c) detail on $[90, 100]$, when red - : deterministic in (a-c), blue -. : SCM in (a,b), and blue: error ε in (c)

$\xi = 0.682$, but a much smaller error of the realization is achieved using the SCM for $\xi = 0.780$.

3.2 Aeroelastic system

3.2.1 Model

With the success of the SCM in the above test models, we now consider applications of SCM for an aeroelastic system. The two-degree-of-freedom dynamic model simulating an airfoil oscillating in pitch and plunge can be expressed as a coupled system of two second-order nonlinear ordinary differential equations, and the detail description can be found in [6]:

$$
\begin{aligned}
&\eta'' + x_\alpha \alpha'' + 2\zeta_\eta \frac{\tilde{\omega}}{U^*}\eta' + \left(\frac{\tilde{\omega}}{U^*}\right)^2 G(\eta) = -\frac{1}{\pi\mu} C_L(\tau) \\
&\frac{x_\alpha}{r_\alpha^2}\eta'' + \alpha'' + 2\frac{\zeta_\alpha}{U^*}\alpha' + \frac{1}{U^{*2}} M(\alpha) = \frac{2}{\pi\mu r_\alpha^2} C_M(\tau).
\end{aligned}
\tag{3.5}
$$

The variable η denotes the non-dimensional plunge displacement, and α is the pitch angle of an airfoil. This is a fluid - structure interaction problem, where the structural terms are given by $M(\alpha)$ and $G(\eta)$, $C_L(\tau)$ and $C_M(\tau)$ represent the aerodynamic terms which are expressed by integral formulations.

Following the procedure proposed in Lee et. al. [6], the integro-differential system (3.5) is transformed into the following eighth-order ODEs. The details of the transformation are given in the Appendix.

$$
\begin{aligned}
x_1' &= x_2 \\
x_2' &= (c_0\mathbf{A} - d_0\mathbf{B})/(d_0c_1 - c_0d_1) \\
x_3' &= x_4 \\
x_4' &= (c_1\mathbf{A} + d_1\mathbf{B})/(d_0c_1 - c_0d_1) \\
x_5' &= x_1 - \epsilon_1 x_5 \\
x_6' &= x_1 - \epsilon_2 x_6 \\
x_7' &= x_3 - \epsilon_1 x_7 \\
x_8' &= x_3 - \epsilon_2 x_8
\end{aligned}
\tag{3.6}
$$

where

$$
\begin{aligned}
\mathbf{A} = d_3x_1 + d_2x_2 + d_5x_3 + d_4x_4 + d_6x_5 + d_7x_6 + d_8x_7 + d_9x_8 \\
+ (\frac{1}{U^*})^2 M(x_1) - g(\tau) \\
\mathbf{B} = c_5x_1 + c_3x_2 + c_4x_3 + c_2x_4 + c_6x_5 + c_7x_6 + c_8x_7 + c_9x_8 \\
+ (\frac{\tilde{\omega}}{U^*})^2 G(x_3) - f(\tau)
\end{aligned}
\tag{3.7}
$$

$$
\begin{aligned}
f(\tau) &= \frac{2}{\mu}((\frac{1}{2} - a_h)\alpha(0) + \eta(0))(\psi_1\varepsilon_1 e^{-\varepsilon_1\tau} + \psi_2\varepsilon_2 e^{-\varepsilon_2\tau}), \\
g(\tau) &= -\frac{(1+2a_h)f(\tau)}{2r_\alpha^2}
\end{aligned}
\tag{3.8}
$$

The nonlinear pitch stiffness term $M(\alpha)$ is defined as a polynomial model, and a linear plunge stiffness term is employed where $G(\eta) = \eta$. The constants $c_0, \ldots, c_9$ and $d_0, \ldots, d_9$ are given in the Appendix. For numerical simulations, the system parameters are specified as follow:

$$
\mu = 100, \quad a_h = -0.5, \quad x_\alpha = 0.25, \quad \tilde{\omega} = 0.2 \quad \text{and} \quad r_\alpha = -0.5 \tag{3.9}
$$

In the present study, the solutions of the eighth-order ODEs are solved by the fourth-order Runge-Kutta integration scheme.

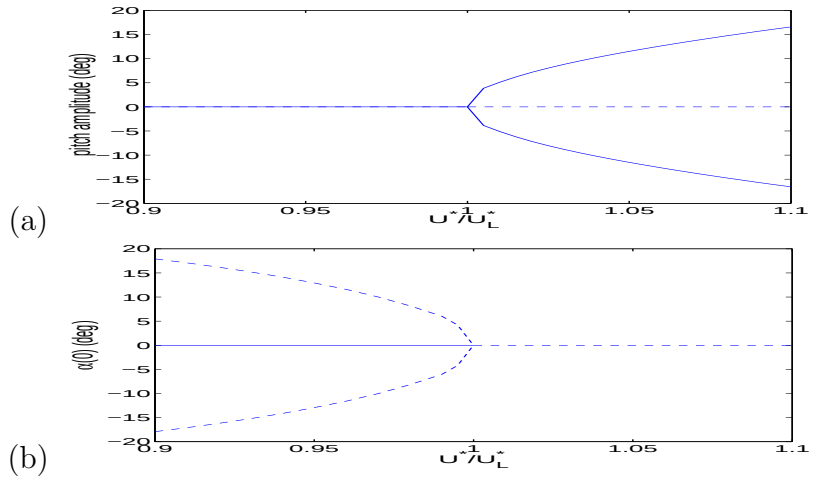

Figure 11: Hopf-bifurcation in the aeroelastic system: solid line: stable branch; dashed line: unstable branch; (a) supercritical bifurcation for $k_3 = 3$; (b) subcritical bifurcation for $k_3 = -3$

If the pitch stiffness term $M(\alpha)$ is given by a cubic polynomial model $M(x_1) = x_1 + k_3 x_1^3$, the aeroelastic system undergoes a Hopf-bifurcation at the $U^* = U_L^*$, where $U_L^* (\approx 6.285)$ is called the linear flutter speed. Here, positive values of k_3 yields a supercritical Hopf bifurcation (see Fig. 11(a)) for which the stable LCO exists for $U^* > U_L^*$; negative values yields a subcritical bifurcation (see Fig. 11(b)) leading to unstable LCO for $U^* < U_L^*$.

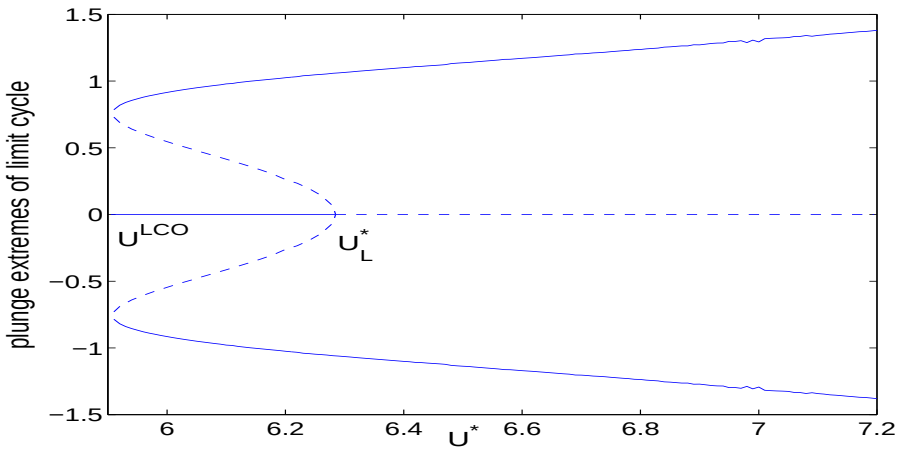

Figure 12: bifurcation diagram for $k_3 = -3$ and $k_5 = 20$: solid line: stable branch; dashed line: unstable branch

In the recent study of Beran et. al.[1], a fifth-order polynomial

$$M(x_1) = x_1 + k_3 x_1^3 + k_5 x^5 \tag{3.10}$$

is employed to model the pitch restoring force. In the situation when $k_3 < 0$ and $k_5 > 0$, there exists a bifurcation point U^{LCO} such that stable LCO exists for $U^{LCO} < U^*$, where $U^{LCO} \approx 5.908$ [1]. Therefore, for $U^{LCO} < U^* < U_L^*$, the aeroelastic system exhibits a stable LCO and an unstable LCO (see Fig. 12). However, for $U^* > U_L^*$, the unstable LCO is fold and only the stable LCO exists in the dynamical system.

3.2.2 LCO I

Consider a fifth-order polynomial (Eq. (3.10)) is used to model the pitch with the coefficient k_5 taken as $k_5 = 20$. The randomness of the aeroelastic system is introduced though uncertainty of the coefficient associated with the cubic term, which is given by

$$k_3(\xi) = [k_3]_0 + [k_3]_1 \xi, \tag{3.11}$$

where $[k_3]_0 = -3$, $[k_3]_1 = 0.2$, and ξ is a uniform random variable on [-4,4]. As the function $f(\tau)$ and $g(\tau)$ can be very close to zero for large values of τ, we set the functions

$g(\tau)$ and $f(\tau)$ to zero. Also the initial condition is first considered as deterministic, where: $x(0) = (0.0147, 0, 0, 0, 0, 0, 0, 0)$.

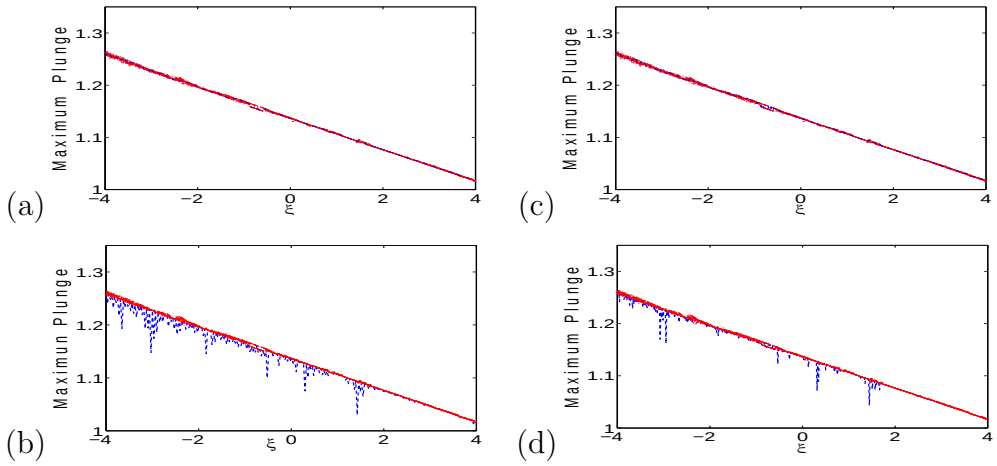

Figure 13: Simulation of maximum plunge values for $U^* = 6.5$:(a,c)$1500 \leq t \leq 2000$, (b,d)$17500 \leq t \leq 18000$ red dots: deterministic; blue dashed lines: SCM with 128 nodes in (a,b), 256 nodes in (c,d)

In order to carry out a reasonable comparison with the results presented in [1], we consider the time domain $t = [0, 18000]$. The time is sufficiently large such that the realization has converged to LCO for t much less than 18000, (actually, the realization converged to LCO at $t < 2000$). Fig.13(a,c) shows the simulations of the maximum plunge values $(x_3(t))$ with respect to ξ when $1,500 < t < 2,000$. Here, the difference of the plunge computed in 2-norm between the SCM and MCS with 4000 samples is only 0.0037 (Fig.13(a) for 128 nodes) and 0.0036 (Fig.13(c) for 256 nodes), which demonstrates that the SCM reproduces the correct LCO for $t < 2000$. To investigate the SCM performance for long-term computations, we compare the plots presented in Fig.13(a) with (b) and (c) with (d). We observe that the error resulting in the decay of the estimated LCO amplitude increase to 0.0306 (Fig.13(b) for SCM with 128 nodes) and 0.0156 (Fig.13(d) for SCM with 256 nodes). Thus, introducing more nodes will enhance the performance of the SCM.

In Fig. 14, we show that the variation of the pitch angle with respect to the random variable ξ for $U^* = 6.5$ (where $U^* > U_L^*$) and $U^* = 6.284$ (where $U^{LCO} < U^* < U_L^*$).

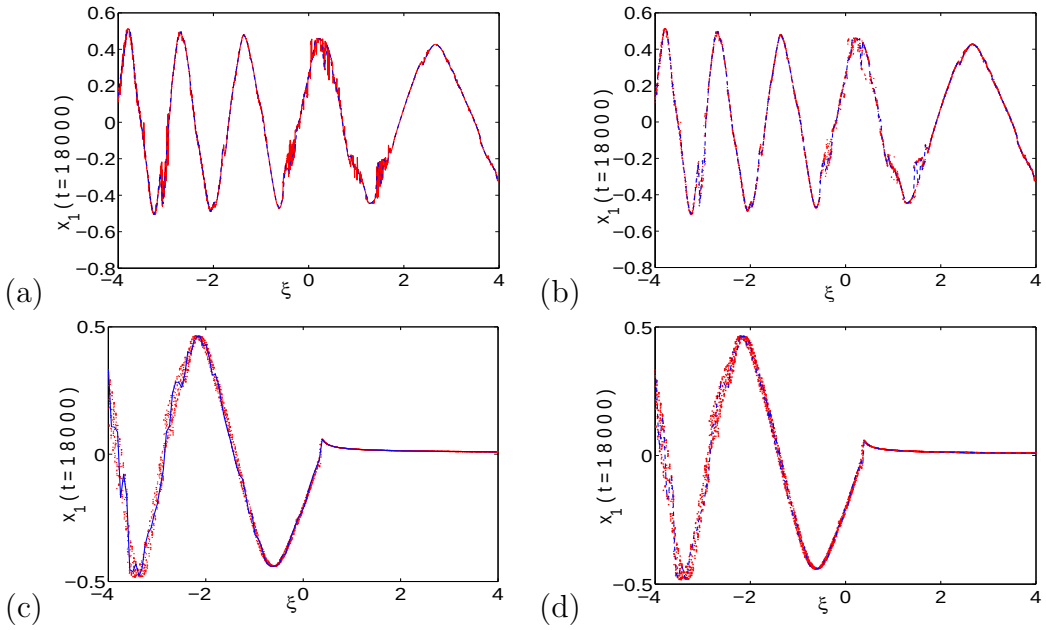

Figure 14: Pitch angle w.r.t the random variable ξ for (a)&(b) $U^* = 6.5$, and (c)&(d) $U^* = 6.284$; with deterministic (red dots) and SCM (blue dashed line) with 128 (in (a,c)) and 256 (in (b,d)) nodes

For the latter case $U^{LCO} < U^* = 6.284 < U_L^*$, an unstable LCO and a stable LCO co-exist, we note that the LCO disappeares at around $\xi = 0.4$ as k_3 increases. The SCM simulations are in good agreement with those deterministic results.

The success of the SCM can also be demonstrated from the probability density function(PDF) of the LCO amplitude. Fig.15 compares the PDF based on the MCS and those using the SCM with 128 and 256 nodes. The stochastic characteristic is well captured by the SCM. When $U^* = 6.284$, we have a bi-modal probability density function as shown in Fig. 15(b). The peak of the density function at zero represents the probability that the system converging to zero, i.e., the probability that the initial point is inside the random unstable LCO; the other peak of the PDF represents the probability that the aeroelastic system converges to a stable LCO.

It is important to note that while the SCM reproduces excellent agreement with the simulation results based on MCS, the SCM is a highly efficient tool to study the stochastic characteristics of the aeroelastic system. The computing time of the SCM

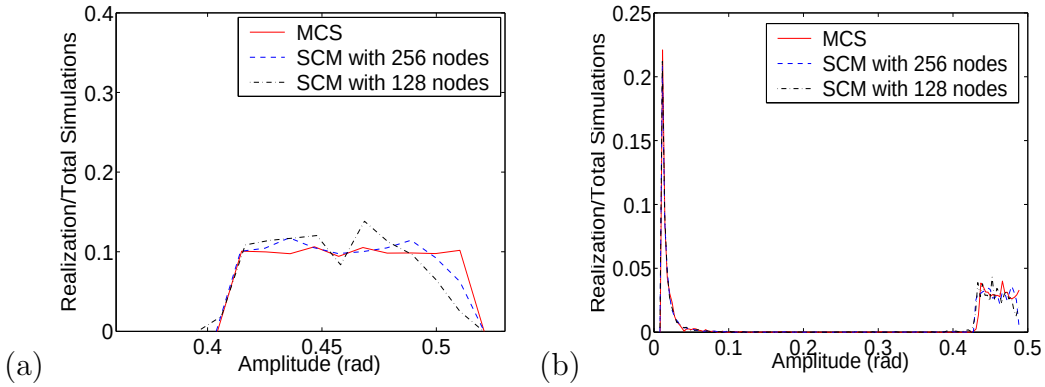

Figure 15: PDFs of amplitude for (a) $U^* = 6.5$, and (b) $U^* = 6.284$

Table 2: CPU time for LCO I t = 18,000

Nodes	4000	128	256
MCS	46849	–	–
SCM	–	1284	2393

is due to the realization on the nodal points. Thus, the computing time for the SCM with 256 nodes is about twice of that needed for the SCM with 128 nodes. However, from Table 1, the computing time for SCM with 256 nodes is only about 5.1% ($\approx \frac{2393}{46849}$) of that required by the MCS with 4000 samples.

3.2.3 LCO II

In the LCO I, we investigate the nonlinear response of the aeroelastic system in the presence of uncertainty in the coefficient of the cubic term in the pitch restoring force. We now extend our study so that the random variables are introduced in the pitch stiffness term and the initial pitch angle. Here, we follow the setting reported in [12], the initial pitch angle $\alpha_0 = \alpha(0)$ and the pitch stiffness term . Notice that, the fifth-order term in pitch restoring force (Eq. (3.10)) $k_5 = 0$. Consider

$$\begin{aligned} k_3(\xi_1) &= [k_3]_0 + [k_3]_1\xi_1 \\ \alpha_0(\xi_2) &= [\alpha_0]_0 + [\alpha_0]_1\xi_2 \end{aligned} \tag{3.12}$$

where $[k_3]_0 = 3.0$ for the hard spring, $[k_3]_1 = 0.3$; $[\alpha_0]_0 = 0.0$, $[\alpha_0]_1 = 0.2$, and ξ_1 and ξ_2 are two independent standard Gaussian random variables. Although the support of the Gaussian distribution is unbounded, we select the nodal points on the interval [-4,4] to include almost all the random input, because for the gaussian density function, we have

$$(\frac{1}{\sqrt{2\pi}})^2 \int_{-4}^{4}\int_{-4}^{4} e^{-1/2(\xi_1^2+\xi_2^2)}\, \mathrm{d}\xi_1 \mathrm{d}\xi_2 \approx 0.9999. \tag{3.13}$$

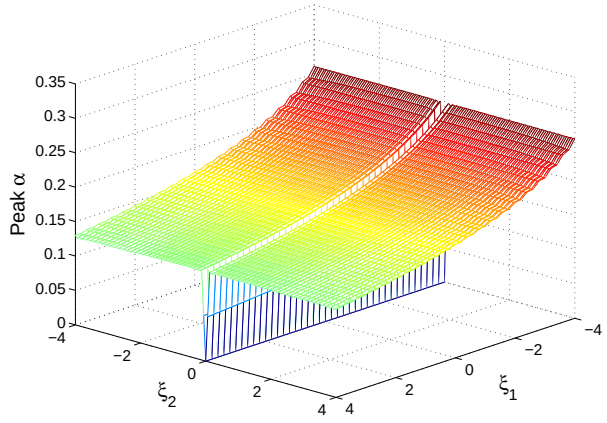

Figure 16: The amplitude response surface for 21×65 tensor nodes

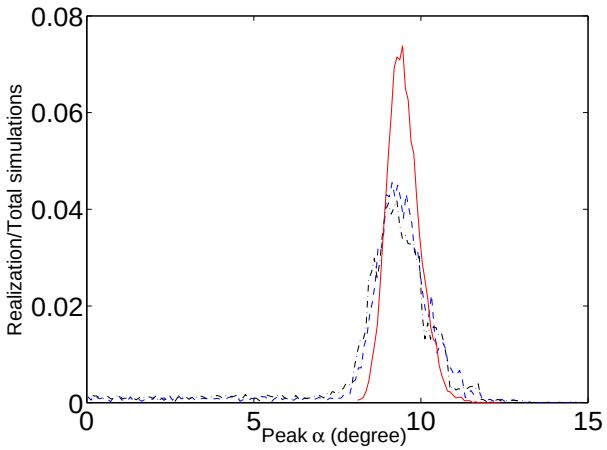

Figure 17: PDFs of the supercritical response at $U^* = 6.5$, red -: MCS; black -.: SCM with 11×51 nodes; blue –: SCM with 21×65 nodes

Here if the initial pitch angle $\alpha(0)$ is not zero, the functions $f(\tau)$ and $g(\tau)$ are reset to (3.8):

The non-dimensional velocity U^* is specified at 6.5. The aeroelastic system is started randomly with the initial point $x(0) = (\alpha_0, 0, 0, 0, 0, 0, 0, 0)$. The time interval $t = [0, 2000]$ is sufficiently large for the system to converge to LCO. The peak α in the last 10% of the time interval is taken as the amplitude of the system. In [12], global polynomial expansion and global Fourier expansion were employed to solve the random differential equation numerically. In this subsection, we will compare the result using the SCM with those based on global polynomial expansion and global Fourier expansion.

The amplitude response surface is shown in Fig. 16. At $\xi_2 = 0$, the system is inactive and there is a concave line on the amplitude response surface. Fig. 17 illustrates the PDF of the LCO amplitude. Notice that the tail of the estimated PDF implies the decay of the amplitude in the SCM simulation. By comparing the results of the SCM with those using the global polynomial expansion and the global Fourier expansion (Fig.6 in [12]), we note that the polynomial chaos expansion fails to capture the range of LCO, and only a slight improvement is observed by increasing the order of the polynomial. We also observe that the peak of the estimated PDF from a tenth-order Fourier chaos expansion is lower than that of SCM, and the tail of the estimated PDF from Fourier chaos expansion is larger than the result from SCM. Therefore, the application of the SCM provides a better prediction to the PDF than the Fourier chaos expansion. In addition, it should be noted that the tenth-order Fourier chaos expansion requires more computing time than the MCS with $10,000$ samples (see Table 2 in [12])

In Fig. 18, we simulate the conditional expected value of ξ_1, $E(x_1(2000, \xi_1, \xi_2)|\xi_2)$, by the MCS with 5000 samples at different fixed values of ξ_2 and by the SCM with 21×65 nodes. The results show the SCM is in excellent agreement with the MCS even near the discontinuity at $\xi_2 = 0$. In contrast, the pitch angle amplitudes for the eighth-order polynomial chaos expansion and the eighth-order Fourier chaos expansion

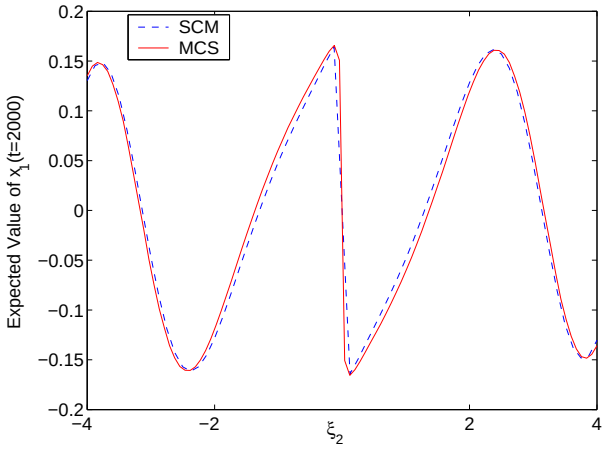

Figure 18: $E[x_1(T;\xi_1,\xi_2)]$ at $T = 2000$ vs ξ_2

Table 3: CPU time for LCO II t=2000

Nodes	10000	11by51	21by65
MCS	10644	–	–
SCM	–	562	1185

are smaller than the MCS in the range of $-1.5 < \xi_2 < 1.5$. In particular, a large tail of the prediction on the PDF of the LCO amplitude is observed for the polynomial chaos expansion [12]. Hence, the discontinuity at $\xi_2 = 0$ causes a serious decay of the simulations for the polynomial chaos expansion and the Fourier chaos expansion.

In Table 2, we display the computing time for LCO II. Even though the number of the nodal points using the SCM increases with the dimension of the random space, significant saving in computing time compared to that required by the MCS is achieved using the SCM.

To study a more complicated case, we consider a fifth-order model for $M(x_1)$ (Eq. (3.10), and let $k_5 = 20$. Moreover the randomness of $k_3(\xi_1)$ and $\alpha_0(\xi_2)$ is as same as that in the previous study. Fig. 19 shows the PDF of the amplitude generated for the hard spring ($k_3 > 0$) and the soft spring ($k_3 < 0$), respectively. Comparing the PDF generated by the SCM with 21×65 nodes (see Fig. 19) with those using the Fourier

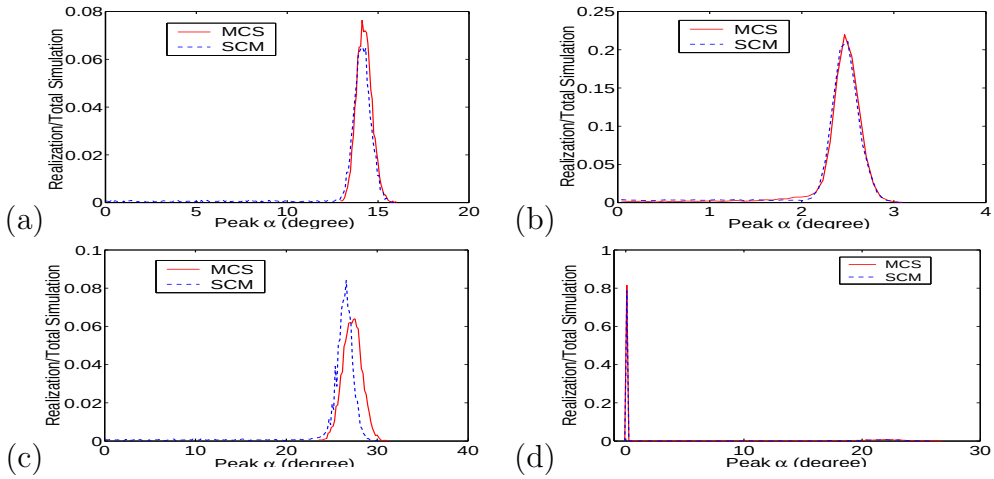

Figure 19: PDFs for (a) $U^* = 6.9$,hard spring and (b) $U^* = 6.3$ hard spring (c) $U^* = 6.6$ soft spring (d) $U^* = 6.0$ soft spring

chaos expansion (see Fig. 8 in [12]), we notice that the SCM has a better prediction of the amplitude. Moreover, it has been reported in Fig. 9 and 11 in [12] that for the soft spring case, the Fourier expansion fails to predict the location of the peak value of the PDF when $U^* \leq 6$. In Fig. 20, we display the location of the peak value of PDF of the LCO amplitude (not including the equilibrium, zero). The estimations from the SCM are in a good agreement with the MCS.

3.2.4 Secondary bifurcation

In the previous subsections (LCO I and LCO II), we studied the Hopf bifurcation and LCO when uncertainty is introduced to an aeroelastic system. We now investigate more complicated cases, namely the secondary bifurcation and the jump phenomenon between the Hopf and secondary bifurcations. The Hopf bifurcation occurs when the flow velocity U^* reaches the linear flutter speed U_L^*. By increasing U^* to about $2U_L^*$, the secondary bifurcation behavior may exist under certain conditions, and this has been investigated by Lee et. al. [5] and Liu et. al. [7]. To study the secondary bifurcation, a strong cubic nonlinearity in the pitch DOF, $M(x_1) = x_1 + k_3 x_1^3$ is usually considered where $k_3 = 80$. Here, the functions given in (3.8)are non-zero.

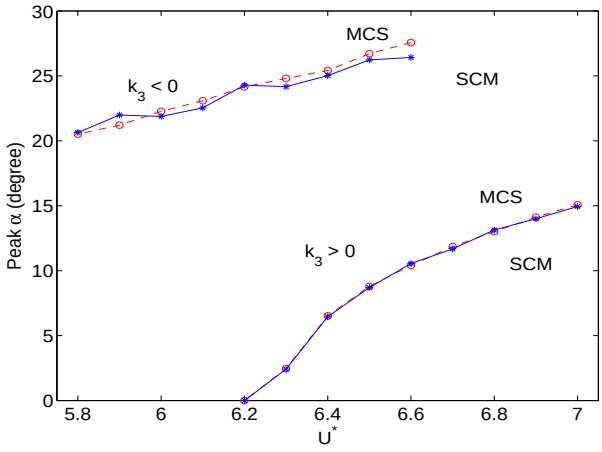

Figure 20: Location of the peak value of PDFs of the LCO amplitude (not including the equilibrium, zero)

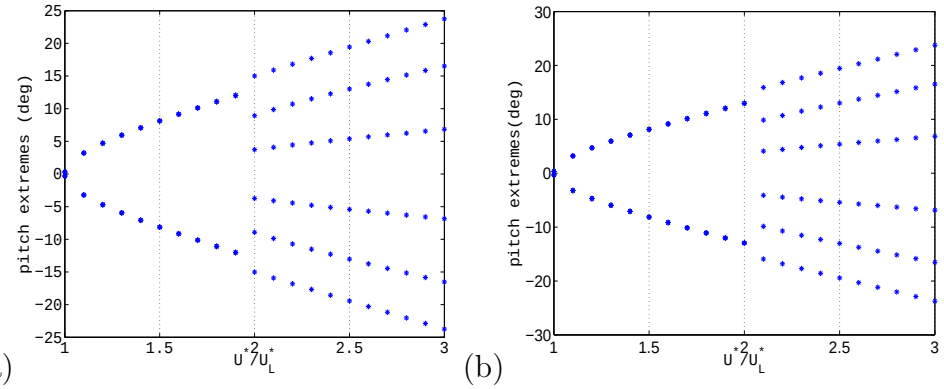

(a) (b)

Figure 21: The extreme pitch with different initial pitch:(a) $\alpha(0) = 1.0°$; (b) $\alpha(0) = 10.0°$

Fig. 21 (a) and (b) show the pitch extreme values versus U^*/U_L^* for the initial pitch angle $\alpha(0) = 1.0°$ and $10.0°$, respectively. From the plot displayed in (a), we observe that the Hopf bifurcation begins at $U^*/U_L^* = 1$, and the secondary bifurcations appears when $U^*/U_L^* = 2$. However, unlike the Hopf bifurcation, the starting point for the secondary bifurcation depends on the initial conditions. When $\alpha(0)$ is $10.0°$, the secondary bifurcation occurs near $U^*/U_L^* = 2.1$.

Liu et. al. ([7]) also note that jump phenomenon in the LCO may exists in which the the pitch motion changes from one positive extreme in the Hopf bifurcation to three positive extremes in the secondary bifurcation. In this thesis, we demonstrate

that similar phenomena exist when a random variable is introduced to the stiffness term in the pitch restoring force. So we will focus on the cases that $U^*/U_L^* \approx 1.98$ in the following studying.

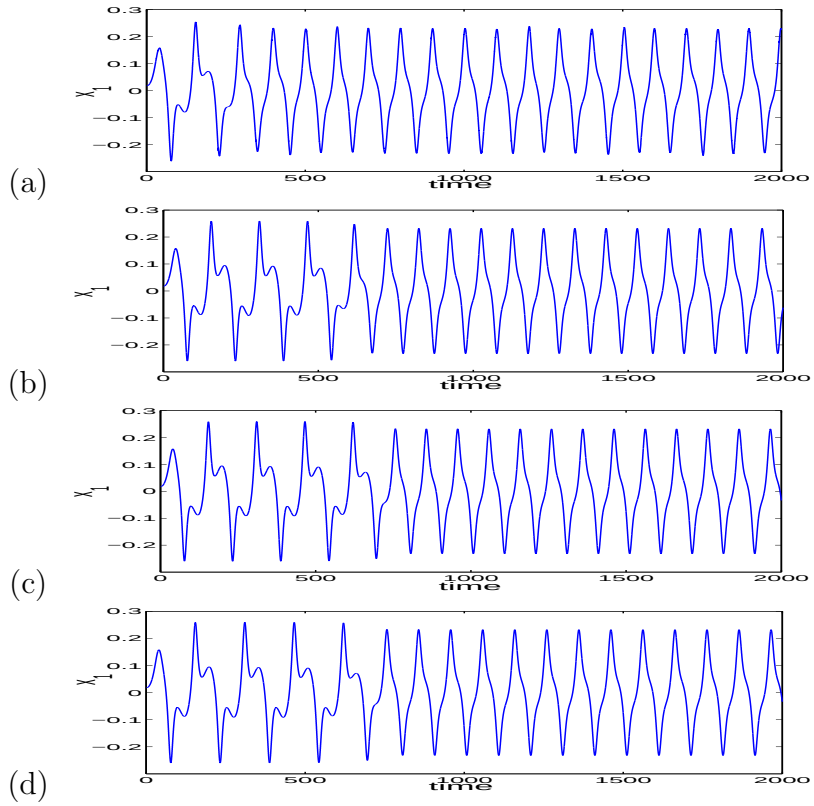

Figure 22: Numerical solution of ode45 for $k_3 = 74$ and $U^*/U_L^* = 1.9803$, the relative and the absolute error tolerance is (a) 10^{-3}; (b)10^{-6}; (c)10^{-11}; (d)10^{-13}

In stochastic analysis, the cubic nonlinearity is used to model $M(x_1) = x_1 + k_3 x_1^3$, and the coefficient for the strong nonlinear term is set as the random variable, where $k_3(\xi) = [k_3]_0 + [k_3]_1 \xi$, where $[k_3]_0 = 80$, $[k_3]_1 = 8$ and ξ is the uniform random variable on $[-1, 1]$. Here, the initial condition is deterministic, $\alpha(0) = 1.0^\circ$ with other initial values set to zero. Near $U^*/U_L^* \approx 1.98$, we observe a jump phenomenon in the pitch motion similar to that reported by Liu et. al. ([7]). However, it is noted that to capture the correct aeroelastic behaviors, a very accurate solver must be employed for the deterministic aeroelastic system. Fig. 22 illustrates the pitch motions using the same ode45 solver, but with different absolute and relative error tolerances. When

the relative and the absolute error tolerence is nongreater than 10^{-11}, the numerical results in Fig. 22 (c,d) is the same. Thus, we consider 10^{-11} is the appropriate value for tolerence and set the relative and the absolute error tolerence to 10^{-11} in the following study.

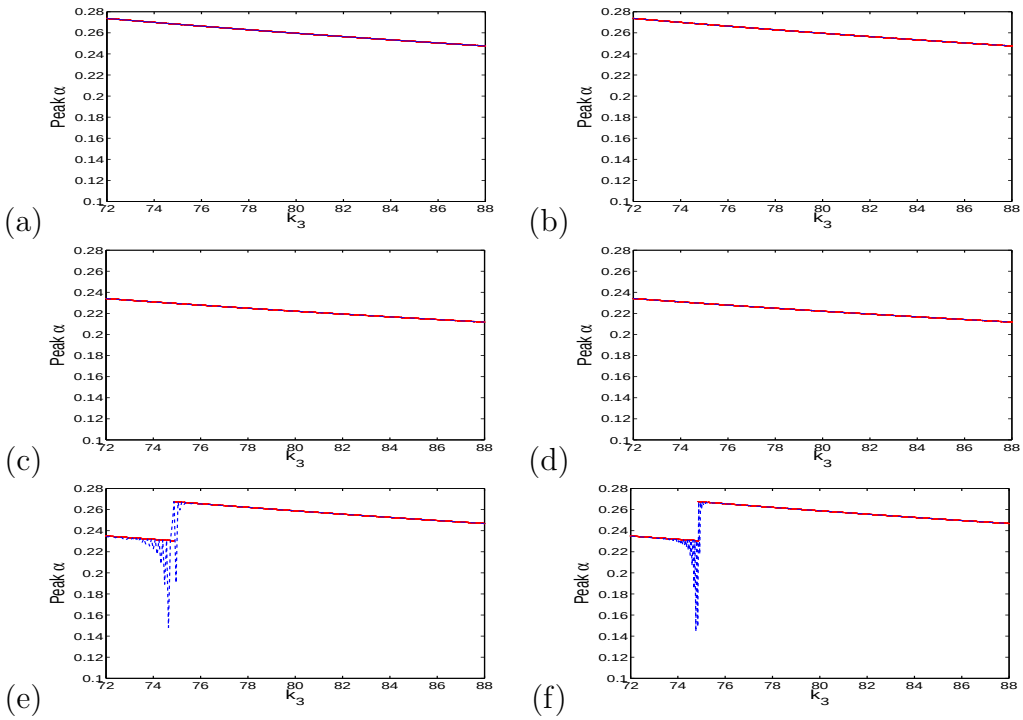

Figure 23: The amplitude response for (a,b) $U^*/U_L = 1.985$; (c,d) $U^*/U_L = 1.975$ and (e,f) $U^*/U_L = 1.9803$; red dots: deterministic, blue dashed lines: SCM with 101 nodes in (a,c,e) and SCM with 201 nodes in (b,d,f)

Fig. 23 shows the LCO amplitude response at different flow velocities. When $U^*/U_L^* = 1.975$ and 1.985 (Fig. 23(a)-(d)), the jump phenomenon of the LCO amplitude does not occur, and the pitch motion is restricted in one type of bifurcation. Notice that, the amplitude for $U^*/U_L^* = 1.985$ (i.e., in the secondary bifurcation) is higher than the amplitude for $U^*/U_L^* = 1.975$ (i.e., in the Hopf bifurcation). However, increasing the flow U^*/U_L^* to 1.9803 (Fig. 23(e,f)), we observe the occurrence of a jump phenomenon in the LCO amplitudes. In Fig. 23(e,f), the LCO amplitude is consists of two discontinuous parts, in which the lower parts corresponds to the Hopf bifurcation and the upper parts corresponds to the secondary bifurcation. It should

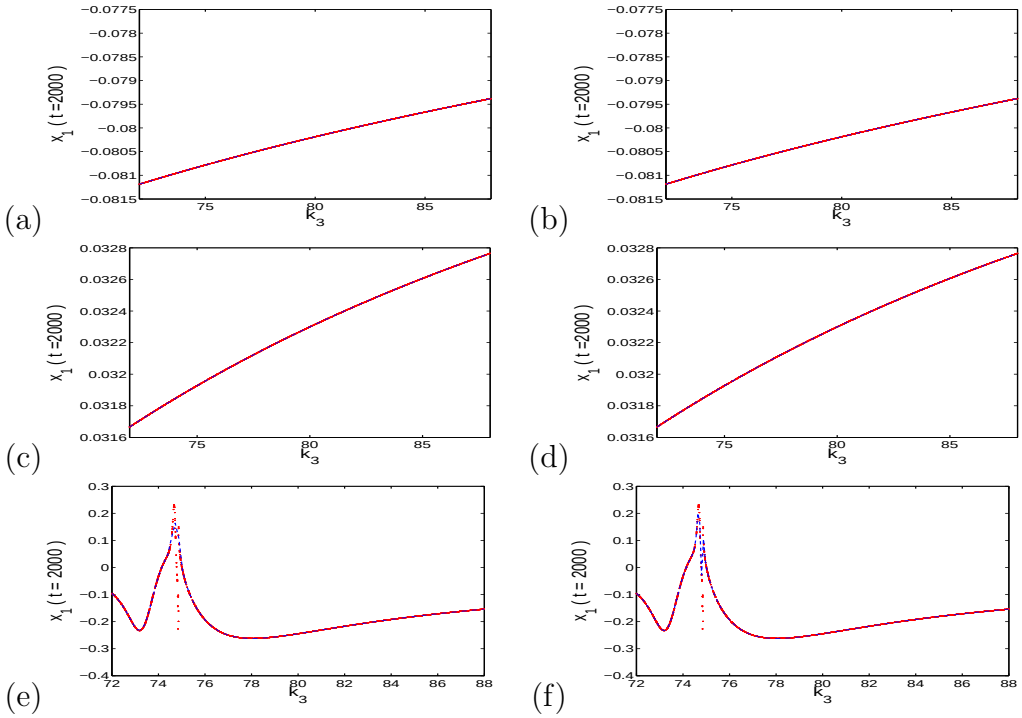

Figure 24: Pitch motion(rad) w.r.t. k_3 for (a,b) $U^*/U_L = 1.985$; (c,d) $U^*/U_L = 1.975$ and (e,f) $U^*/U_L = 1.9803$; red dots: deterministic, blue dashed lines: SCM with 101 nodes in (a,c,e) and SCM with 201 nodes in (b,d,f)

be noted that in this study, the initial condition is fixed, and the jump phenomenon at $U^*/U_L^* = 1.9803$ occurs near $k_3 = 75$.

The simulation results using the SCM at $U^*/U_L^* = 1.9803$ are displayed in Fig. 23 (e,f). It clearly shows that there are significant decay of the amplitudes near $k_3 = 75$, at which the jump phenomenon between the bifurcations occurred. The jump phenomenon between the bifurcation increases the difficulty for the SCM to simulate the LCO amplitude of the aeroelastic system. However, the serious decay around the discontinuity can be reduced by including more nodes in the SCM. In Fig. 23 (a-d), we also observe that no decay in the amplitudes are noticed for $U^*/U_L^* = 1.975$ and 1.985, in which the pitch motion is entirely in Hopf or the secondary bifurcation.

As discussed above, the decay of amplitude is produced due to the error of the interpolation in the random space. The simulated pitch motion at $x_1(t = 2000, k_3)$ for the three flow velocities are shown in Fig. 24. Here, we notice that the significant

delay of the amplitude simulation happens around the particular value of k_3 in which the pitch motion is discontinuous in the random space. The results presented in Fig. 24 reconfirm the simulation reported in Fig. 23.

It would be of interest to investigated the jump phenomenon when considering that random variables are present not only in the pitch restoring force, but also in the initial condition and the flow velocity.

Acknowledgement

Our work made use of the infrastructure and resources of AICT (Academic Information and Communication Technologies) of the University of Alberta.

Chapter 4

Conclusions

Stochastic collocation method is an algorithm in which the estimation is based on the interpolation at different time steps. In this thesis, the SCM is developed for dynamical systems with random parameters. Numerical simulations have been carried out to demonstrate the SCM is much more efficient than the MCS. Moreover, by investigating the UQ problems dealing with a long time simulation or with a discontinuity in the random space as reported in [1] - [12], and comparing the results obtained by the global chaos expansion, the SCM has consistently shown a better performance than the global chaos expansion, such as Polynomial chaos expansion and Fourier chaos expansion. We also compare the SCM with the DWT, and the performance of SCM is at least as good as that of DWT. However, it should be pointed out that the SCM requires less computing time that the DWT since the coefficients are not generated from the wavelet basis. Another attractive feature of the SCM is that it is straightforward and easy to implement to various UQ problems.

However, the SCM can not completely overcome difficulties of the UQ problems with long time integration. The estimated expectation from SCM suffers loss of accuracy after a long time simulation, and more nodes are required to retain the accuracy. In our current study, the nodal points are selected at the beginning of the computation and remain unchanged in the time domain. Therefore, it would be desirable to develop an adaptive algorithm, so that the number of nodes and their selection are adjusted at different time steps. The difficulty with this approach is that the coefficients of the Lagrange polynomial is hard to evolve in multidimensional cases. Even though the tensor product can be used to construct SCM in multidimensional UQ problems,

the number of nodes will increase exponentially in order to retain the accuracy as the dimension of the random space increases. Consequently, it makes the computational time unacceptable large in multidimensional cases. Thus, the SCM is mostly preferred for UQ problems in the lower dimensions.

In this thesis, we focused on the the random differential equations, and the results clearly demonstrate that the SCM is an efficient numerical tool to study RDEs. However, the usage of the SCM is restricted to RDE, and it is not applicable to stochastic differential equations.

Appendix A

Transformation of aeroelastic system

The 2 DOF oscillating in pitch and plunge aeroelastic system is expressed as [6]:

$$\begin{aligned} \eta'' + x_\alpha \alpha'' + 2\zeta_\eta \frac{\tilde{\omega}}{U^*}\eta' + \left(\frac{\tilde{\omega}}{U^*}\right)^2 G(\eta) &= -\frac{1}{\pi\mu}C_L(\tau) \\ \frac{x_\alpha}{r_\alpha^2}\eta'' + \alpha'' + 2\frac{\zeta_\alpha}{U^*}\alpha' + \frac{1}{U^{*2}}M(\alpha) &= \frac{2}{\pi\mu r_\alpha^2}C_M(\tau), \end{aligned} \tag{A.1}$$

where η is the non-dimensional plunge displacement of the elastic axis; α is the pitch angle of an airfoil; r_α is the radius of gyration about the elastic axis; μ is the mass ratio given by

$$\mu = m/\pi\rho b^2, \tag{A.2}$$

where m is the mass of the airfoil; ρ is the freestream density and b is the airfoil semi-chord.

U^* is the non-dimensional velocity and $\tilde{\omega}$ is the frequency ratio defined as

$$U^* = U/b\omega_\alpha \tag{A.3}$$

$$\tilde{\omega} = \omega_\eta/\omega_\alpha, \tag{A.4}$$

where U is the free-stream velocity and ω_α and ω_η are the uncoupled plunging and pitching modes natural frequencies. The differentiation is with respect to the non-dimensional time τ defined as

$$\tau = Ut/b \tag{A.5}$$

$C_L(\tau)$ and $C_M(\tau)$ in (3.5) are the lift and pitching moment coefficients, respectively. They are expressed as:

$$\begin{aligned} C_L(\tau) =&\pi(\eta'' - a_h\alpha'' + \alpha') + 2\pi\{\alpha(0) + \eta'(0) + [\frac{1}{2} - a_h]\alpha'(0)\}\phi(\tau) \\ &+ 2\pi\int_0^\tau \phi(\tau-\sigma)[\alpha'(\sigma) + \eta''(\sigma) + (\frac{1}{2} - a_h)\alpha''(\sigma)]\mathrm{d}\sigma, \end{aligned} \tag{A.6}$$

$$\begin{aligned} C_M(\tau) =&\pi(\frac{1}{2} + a_h)\{\alpha(0) + \eta'(0) + [\frac{1}{2} - a_h]\alpha'(0)\}\phi(\tau) \\ &+ \pi(\frac{1}{2} + a_h)\int_0^\tau \phi(\tau-\sigma)[\alpha'(\sigma) + \eta''(\sigma) + (\frac{1}{2} - a_h)\alpha''(\sigma)]\mathrm{d}\sigma \\ &+ \frac{\pi}{2}a_h(\eta'' - a_h\alpha'') - (\frac{1}{2} - a_h)\frac{\pi}{2}\alpha' - \frac{\pi}{16}\alpha'' \end{aligned} \tag{A.7}$$

where the Wagner's function $\phi(\tau)$ is given by

$$\phi(\tau) = 1 - \psi_1 e^{-\varepsilon_1\tau}\psi_2 e^{-\varepsilon_2\tau} \tag{A.8}$$

and the constants are $\psi_1 = 0.165$, $\psi_2 = 0.335$, $\varepsilon_1 = 0.0455$ and $\varepsilon_2 = 0.3$.

By introducing four new variables w_1, w_2, w_3, w_4:

$$w_1(\tau) = \int_0^\tau e^{-\varepsilon_1(\tau-\sigma)}\alpha(\sigma)\mathrm{d}\sigma$$

$$w_2(\tau) = \int_0^\tau e^{-\varepsilon_2(\tau-\sigma)}\alpha(\sigma)\mathrm{d}\sigma$$

$$w_3(\tau) = \int_0^\tau e^{-\varepsilon_1(\tau-\sigma)}\eta(\sigma)\mathrm{d}\sigma$$

$$w_4(\tau) = \int_0^\tau e^{-\varepsilon_2(\tau-\sigma)}\eta(\sigma)\mathrm{d}\sigma$$

, (A.1) can be rewritten as:

$$\begin{aligned} &c_0\eta'' + c_1\alpha'' + c_2\eta' + c_3\alpha' + c_4\eta + c_5\alpha + c_6w_1 + c_7w_2 + c_8w_3 + c_9w_4 \\ &+ (\frac{\tilde{\omega}}{U^*})^2 G(\eta) = f(\tau) \\ &d_0\eta'' + d_1\alpha'' + d_2\eta' + d_3\alpha' + d_4\eta + d_5\alpha + d_6w_1 + d_7w_2 + d_8w_3 + d_9w_4 \\ &+ (\frac{1}{U^*})^2 M(\alpha) = g(\tau). \end{aligned} \tag{A.9}$$

The coefficients of equation (A.9) are as follows:

$$c_0 = 1 + \frac{1}{\mu}, \quad c_1 = x_\alpha - \frac{a_h}{\mu}, \quad c_2 = 2\zeta_\eta \frac{\tilde{\omega}}{U^*} + \frac{2}{\mu}(1 - \psi_1 - \psi_2),$$

$$c_3 = \frac{1 + (1 - 2a_h)(1 - \psi_1 - \psi_2)}{\mu}, \quad c_4 = \frac{2}{\mu}(\psi_1\varepsilon_1 + \psi_2\varepsilon_2),$$

$$c_5 = \frac{2}{\mu}[(1 - \psi_1 - \psi_2) + (1/2 - a_h)(\psi_1\varepsilon_1 + \psi_2\varepsilon_2)],$$

$$c_6 = \frac{2}{\mu}\psi_1\varepsilon_1[1 - (1/2 - a_h)\varepsilon_1], \quad c_7 = \frac{2}{\mu}\psi_2\varepsilon_2[1 - (1/2 - a_h)\varepsilon_2],$$

$$c_8 = -\frac{2}{\mu}\psi_1\varepsilon_1^2, \quad c_9 = -\frac{2}{\mu}\psi_2\varepsilon_2^2,$$

$$d_0 = \frac{x_\alpha}{r_\alpha^2} - \frac{a_h}{\mu r_\alpha^2}, \quad d_1 = 1 + \frac{1 + 8a_h^2}{8\mu r_\alpha^2},$$

$$d_2 = 2\frac{\zeta_\eta}{U^*} + \frac{1 - 2a_h}{2\mu r_\alpha^2} - \frac{(1 + 2a_h)(1 - 2a_h)(1 - \psi_1 - \psi_2)}{2\mu r_\alpha^2},$$

$$d_3 = -\frac{(1 + 2a_h)(1 - \psi_1 - \psi_2)}{\mu r_\alpha^2} - \frac{(1 + 2a_h)(1 - 2a_h)(\psi_1\varepsilon_1 + \psi_2\varepsilon_2)}{2\mu r_\alpha^2},$$

$$d_4 = -\frac{(1 + 2a_h)(1 - \psi_1 - \psi_2)}{\mu r_\alpha^2}, \quad d_5 = \frac{(1 + 2a_h)(1 - 2a_h)(\psi_1\varepsilon_1 + \psi_2\varepsilon_2)}{2\mu r_\alpha^2},$$

$$d_6 = -\frac{(1 + 2a_h)\psi_1\varepsilon_1[1 - (1/2 - a_h)\varepsilon_1]}{\mu r_\alpha^2} \quad d_7 = -\frac{(1 + 2a_h)\psi_2\varepsilon_2[1 - (1/2 - a_h)\varepsilon_2]}{\mu r_\alpha^2},$$

$$d_8 = -\frac{(1 + 2a_h)\psi_1\varepsilon_1^2}{\mu r_\alpha^2}, \quad d_9 = -\frac{(1 + 2a_h)\psi_2\varepsilon_2^2}{\mu r_\alpha^2},$$

where $M(\alpha)$ is the nonlinear pitch stiffness term, $G(\eta) = \eta$ is the linearity plunge stiffness term.

Let $x_1 = \alpha, x_2 = \alpha', x_3 = \eta, x_4 = \eta', x_5 = w_1, x_6 = w_2, x_7 = w_3$, and $x_8 = w_4$. we can rewrite (A.9) as the following eight-order ODE.

$$\begin{aligned}
x_1' &= x_2 \\
x_2' &= (c_0\mathbf{A} - d_0\mathbf{B})/(d_0c_1 - c_0d_1) \\
x_3' &= x_4 \\
x_4' &= (c_1\mathbf{A} + d_1\mathbf{B})/(d_0c_1 - c_0d_1) \\
x_5' &= x_1 - \epsilon_1 x_5 \\
x_6' &= x_1 - \epsilon_2 x_6 \\
x_7' &= x_3 - \epsilon_1 x_7 \\
x_8' &= x_3 - \epsilon_2 x_8,
\end{aligned} \tag{A.10}$$

where

$$\begin{aligned}
\mathbf{A} = d_3x_1 + d_2x_2 + d_5x_3 + d_4x_4 + d_6x_5 + d_7x_6 + d_8x_7 + d_9x_8 \\
+ (\frac{1}{U^*})^2 M(x_1) - g(\tau), \\
\mathbf{B} = c_5x_1 + c_3x_2 + c_4x_3 + c_2x_4 + c_6x_5 + c_7x_6 + c_8x_7 + c_9x_8 \\
+ (\frac{\tilde{\omega}}{U^*})^2 G(x_3) - f(\tau).
\end{aligned} \tag{A.11}$$

Bibliography

[1] P.S. Beran, C.L. Pettit, and D.R. Millman. Uncertainty quantification of limit-cycle oscillations. *Journal of Computational Physics*, 217(1):217–244, 2006.

[2] Chsistian Houdré and Victor Pérez-Abreu. *Chaos expansions, multiple Wiener-Ito integrals and their applications*. CRC Press, 1994.

[3] John K. Hunter and Bruno Nachtergaele. *Applied analysis*. World Scientific, 2001.

[4] I.S.Berezin and N.P.Zhidkov. *Computing Method*. Pergamon Press, 1965.

[5] Lee B. H. K., L. Liu, and K. W Chung. Airfoil motion in subsonic flow with strong cubic nonlinear restoring forces. *Journal of Sound and Vibration*, 281(3-5):483–1245, 2004.

[6] B. H. K. Lee, S. J. Price, and Y. S. Wong. Nonlinear aeroelastic analysis of airfoils: bifurcation and chaos. *Progress in Aerospace Sciences*, 35:205–334, 1999.

[7] Liping Liu and Earl H.Dowell. The secondary bifurcation of an aeroelastic airfoil motion: Effect of high harmonics. *Nonlinear Dynamics*, (37):31–49, 2004.

[8] O.P.Le Maitre, O.M.Knio, H.N.Najm, and R.G.Ghanem. Uncertainty propagation using wiener-haar expansions. *Journal of Computational Physics*, pages 28–57, 2004.

[9] Stephane Mallat. *A Wavelet Tour of Signal Processing*. Academic Press, second edition.

[10] Bernt Oksendal. *Stochastic Differential Equations: An Introduction with Applications*. Springer-Verlag, sixth edition.

[11] C.L. Pettit and P.S. Beran. Spectral and multiresolution wiener expansions of oscillatory stochastic processes. *Journal of Sound and Vibration*, 294(4-5):752–779, 2006.

[12] D.R. Millman P.I.King and P.S. Beran. Airfoil pitch-and-plunge bifurcation behavior with fourier chaos expansions. *Journal of Aircraft*, 42(2):376–384, 2005.

[13] R.G.Ghanem and P.Spanos. *Stochastic Finite Elements:a Spectral Approach.* Springer-Verlag, 1991.

[14] Cyganowski. Sasha, Kloeden. Peter, and Ombach. Jerzy. *From Elementary Probability to Stochastic Differential Equations with MAPLE.* Springer, Berlin ; New York, 2002.

[15] Christoph W. Ueberhuber. *Numerical Computation Methods, Software, and Analysis.* Springer, 1995.

[16] M.M.R. Williams. Polynomial chaos functions and stochastic differential equations. *Annals of Nuclear Energy*, 33:774–785, 2006.

[17] D. Xiu X, Wan and G.E.Karniadakis. Stochastic solution for the two dimensional advection-diffusion equation. *SIAM J. SCI. COMPUT.*, 26(2):578–590, 2004.

[18] G.E. Karniadakis X. Wan. An adaptive multi-element generalized polynomial chaos methods for stochastic differential equations. *Journal of Computational Physics*, 209:617–642, 2005.

[19] G.E. Karniadakis X. Wan. Long-term behavior of polynomial chaos in stochastic flow simulation. *Computer method in applied mechanics and enginerring*, 195(41-43):5582–5596, 2006.

[20] D. Xiu and J. S. Hesthaven. High-order collocation methods for differential equation with random inputs. *SIAM J.Sci.Comput.*, 27(3):1118–1139, 2005.

[21] Dongbin. Xiu. Fast numerical methods for stochastic computations: A review. *Commum. Comput. Phys.*, 5(2-4):242–272, 2009.

[22] Dongbin. Xiu and George E. Karniadakis. The wiener-askey polynomial chaos for stochastic differential equations. *SIAM J. SCI. COMPUT.*, 24(2):619–644, 2002.